Young Scientists Workshop 2007

Book of Abstracts

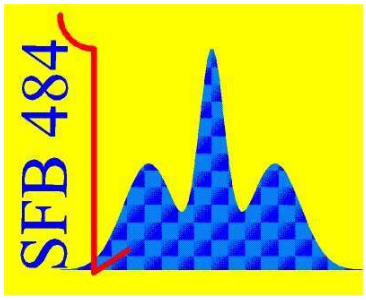

Reimlingen

June 07-10, 2007

Organization:
Alexander Krimmel and Peter Schwab
Institut für Physik
Universität Augsburg

Contents

1 Program

Thursday, June 7, 2007

10:27		Leave from Augsburg station
11:33		Arrival at Nördlingen station.
		Bus transfer to Reimlingen
12:30		Check-in at Bildungshaus St. Albert
13:00		Lunch
14:15	Alexander Krimmel, Peter Schwab	Welcome
14:30 - 15:20	Michael Krispin	Preparation and characterization of Fe- and Co-oxide nanoparticles
15:20 - 16:10	Florian Schrettle	Multiferroic phases in $Eu_{1-x}Y_xMnO_3$
16:10 - 16:40		Coffee
16:40 - 17:30	Cosimo Gorini	Transport theory beyond the Boltzmann equation: the quasiclassical approach
17:30 - 18:20	Michal Sentef	Magnetization transport in 2D and 3D Heisenberg antiferromagnets
19:00		Dinner

Friday, June 8, 2007

08:00		Breakfast
09:00 - 09:50	Christian Kant, Thorsten Rudolf	Infrared spectroscopy on chromium spinels
09:50 - 10:40	Robert Hager	Kondo effect in low carrier systems
10:40 - 11:10		Coffee
11:10 - 11:45	Rosiana Aguiar	Oxynitride perovskites
11:45 - 12:20	Stefan Riegg	Magnetic and electrical transitions in La_2RuO_5
13:00		Lunch
afternoon		Trip to Nördlingen
19:00		Dinner

Saturday, June 9, 2007

08:00		Breakfast
09:00 - 09:50	Franz Josef Kaiser	Coulomb repulsion effects in driven electron transport
09:50 - 10:40	Stefan Schenk	Density functional theory for lattice models
10:40 - 11:10		Coffee
11:10 - 12:00	Stefan Krohns	Colossal dielectric constants and muliferroic behaviour
12:00 - 12:50	Günter Obermeier	Metal-insulator-transition of V_2O_3 in thin films investigated by surface acoustic waves
13:00		Lunch
14:30 - 15:20	Hyun-Jung Lee	Numerical renormalization group calculations for impurity quantum phase transitions
15:20 - 16:10	Alexej Pashkin	Pressure dependence of the low-dimensional compounds TiOCl and TiOBr
16:10 - 16:40		Coffee
16:40 - 17:20	Kaneez Rabia	Pressure-dependent IR-UV spectroscopy on the spin-chain and spin-ladder system $(Sr,Ca)_{14}Cu_{24}O_{41}$
19:00		Dinner

Sunday, June 10, 2007

08:00		Breakfast
09:00 - 09:50	Mamoun Hemmida	Electron spin resonance in two-dimensional magnets
09:50 - 10:40	Martin Eckstein	Thermalization in quantum many-particle systems
10:40 - 11:10		Coffee
11:00 - 11:30	Alexander Krimmel, Peter Schwab	Closing remarks
12:00		Lunch
13:00		Bus transfer to Nördlingen station
15:28		Arrival at Augsburg

2 Rosiana Aguiar: Oxynitride Perovskites

Perovskite-type oxides display a very large range of structural, physical and chemical properties. Due to the flexibility of the perovskite structure it is possible to make substitutions with cations of different size, formal charge and electronegativity, forming solid solutions with gradual or sudden changes in their properties. While cationic substitutions in perovskites have been intensively studied for decades comparatively little is know about substitutions in the anion lattice. Partial replacement of oxygen by nitrogen leads to oxynitrides of general composition $ABO_{3-x}N_x$. The lower electronegativity of nitrogen compared to oxygen results in an increase in the covalence of bonding when nitrogen is inserted in the anionic sublattice. In many cases the optical band gap is reduced to the visible region leading to intensively colored compounds. This intrinsic property of the oxynitride perovskite makes them good candidates to be employed as environmental friendly pigments and photocatalysts [1]. It is possible to tailor the band gaps of oxynitride perovskites, and in turn adjust their colours, by conscious cationic substitution. In oxynitrides of the composition ABO_2N the band gap can be decreased by increasing the crystallographic symmetry (i.e. adjusting the size of the A cation) or by increasing the electronegativity of the B cation [2]. Special kinds of oxynitride perovskite are the ones that contain B-cation with partly filled d-orbitals. The ammonolysis of these systems results in a change of the oxidation state of the B-cation, yielding new compounds, which in some cases exhibit exceptional magnetic or electric properties. For example, $SrMoO_4$ was reacted with ammonia at 800C for 11, 48 and 72 hours, the obtained samples were $SrMoO_{1.95(5)}N_{1.05(5)}$, $SrMoO_{1.81(5)}N_{1.19(5)}$ and $SrMoO_{1.73(5)}N_{1.27(5)}$, respectively. The measured O/N content corresponds to a mixed oxidation state between +5/+6 for molybdenum, specifically +5.03 for $SrMoO_{1.95(5)}N_{1.05(5)}$ and +5.19 for $SrMoO_{1.81(5)}N_{1.19(5)}$. The Seebeck coefficient of the samples increases with nitrogen content while on the other hand electrical conductivity decreases. Contrary to the metallic $SrMoO_3$ the electrical conductivity of the oxynitrides increases with temperature, i.e. a semiconducting behavior is observed [3]. In many applications it is necessary to use thin layers. Thin films of the perovskite system $La_xSr_{(1-x)}TiO_{3+x/2}$ were grown by spin coating technique and by pulsed laser deposition (PLD). The films were subsequent ammonolysis, resulting in the oxynitrides $La_xSr_{1-x}Ti(O,N)_3$. In contrast to the transparent oxide films, the corresponding oxynitrides are coloured. The majority of the films grown by PLD are epitaxially to the (100) direction of cubic perovskite, while the films grown by spin coating possessed no preferential orientation. In general the samples produced by PLD have lower electrical resistivity than the ones grown by spin coating, probably due to the denser structure of the PLD films [4, 5]. Oxynitride single crystalline layers, with general formula ABO_2N (A = La, Sr, Nd and B = Ti, Ta) were synthesized by ammonolysis of respective oxide single crystals. The nitridation of the crystals results in a dramatic change in colour. Optical spectroscopy revealed shifts of the absorption edge by more than 200 nm to longer wavelengths with respect to the parent oxides, corresponding to a reduction of the band gap energies by 1.4-1.8 eV [6].

[1] R. Aguiar, Y. Lee, K. Domen, A. Kalytta, D. Logvinovich, A. Weidenkaff, A. Reller, and S. G. Ebbinghaus, Ceramic Materials Research Trends (2007), in press.

[2] R. Aguiar, D. Logvinovich, A.Weidenkaff, A. Reller, and S. G. Ebbinghaus, Dyes and Pigments (2007), in press, doi:10.1016/j.dyepig.2006.08.029

[3] D. Logvinovich, R. Aguiar, R. Robert, M. Trottmann, S.G. Ebbinghaus, A. Reller, and A. Weidenkaff, submitted to J. Sol. J. Solid State Chem.

[4] R. Aguiar, D. Logvinovich, A. Weidenkaff, H. Karl, C. W. Schneider, A. Reller, and S. G. Ebbinghaus, Mat. Res. Bul. (2007), accepted.

[5] R. Aguiar, A. Weidenkaff, C. W. Schneider, A. Reller, and S. G. Ebbinghaus, Prog. Solid State Chem. (2007), in press, doi: 10.1016/j.progsolidstchem.2007.01.033

[6] S. G. Ebbinghaus , R. Aguiar , A. Weidenkaff, S. Gsell, and A. Reller, Sol. State Sci. (2007), in press, doi:10.1016/j.solidstatesciences.2007.03.011

3 Martin Eckstein: Thermalization in Quantum Many-Particle Systems

How does a correlated quantum-mechanical many-body system behave after it is quenched out of thermal equilibrium? Full thermalization implies the loss of all information about the initial state, which seems to be in conflict with the reversibility of mechanics. To resolve this apparent paradox Boltzmann introduced the ergodic hypothesis [1], which bases the statistical behavior of *closed* systems on the complexity of their dynamics, rather than on the coupling to the environment. However, the ergodic hypothesis has been prooven only for very simple model systems so far. Thus the thermalization of closed systems remains an interesting topic as well for experimental as for theoretical studies, which are discussed in this talk.

Due to their excellent isolation from environment and the perfect control over almost all parameters, ultracold atoms form an ideal medium for the investigation of both equilibrium properties and dynamics of quantum-mechanical many-body systems. E.g., Kinoshita et al. [2] studied a Bose-gas in an one-dimensional optical trap; the atom cloud was split into two parts oszillating against each other, but no thermalization could be observed even after 40 oszillation periods. On the other hand, in solid-state systems there are always many different interactions present and isolation from environment is hardly possible. However, various processes take place on very different time-scales and may thus be observed almost independently. Thermalization of the electron-gas in gold, e.g., takes place on a time-scale of femtoseconds on which the energy exchange with the lattice plays a minor role. It can be analyzed with time-dependent photoemission spectroscopy [3].

Theoretically, it is easy to see that thermalization is impossible in a non-interacting system because the occupation of the single-particle eigenstates cannot change. The situation is similar for *integrable* systems, i.e., when there exist as many integrals of motion as degrees of freedom. Conservation of all those quantities after a quench imposes a constraint that is incompatible with the development of a thermal state [4]. This may explain the absence of thermalization in the one-dimensional Bose gas mentioned above [2, 4]. On the other hand, the recent development of time-dependent Dynamical Matrix Renormalization Group (DMRG) made numerical investigations of large one-dimensional *non-integrable* systems possible. For spinless fermions (with next-nearest neighbor interaction) [5] one finds relaxation to a non-thermal steady state after a sudden change of the interaction. The lack of thermalization can thus be unrelated to integrability. However, in numerical analysis neither infinite particle number nor infinite times after the quench are accessible. This requires some caution in the interpretation of results, in particular in view of the peculiar behavior that has been found in classical non-integrable systems like the Fermi-Fasta-Ulam problem [6].

Complementary to numerical studies of finite-dimensional and finite-size systems, Dynamical Mean-field theory (DMFT) can be used to investigate systems directly in the thermodynamic limit. This theory, which is exact in the limit of infinite spacial dimensions, has become an important method for the investigation of correlated many body systems in equilibrium during the last 15 years. In principle it is also applicable to non-equilibrium situations, but except for few cases it has not been done due to large numerical effort [7]. In the last part of this talk we discuss an interaction-quench in the homogeneous phase of the Falicov-Kimball model, which can be treated analytically within DMFT. The Falicov-Kimball model describes fermions with two different flavors an a lattice, which interact trough a local Coulomb repulsion. Only one flavor can hop on the lattice whereas the other one is considered as immobile. In Fig. 3 we plot the occupation of momentum states (more precisely, the single-particle states of the noninteracting part of the Hamiltonian) in the thermal state before, and in the stationary state

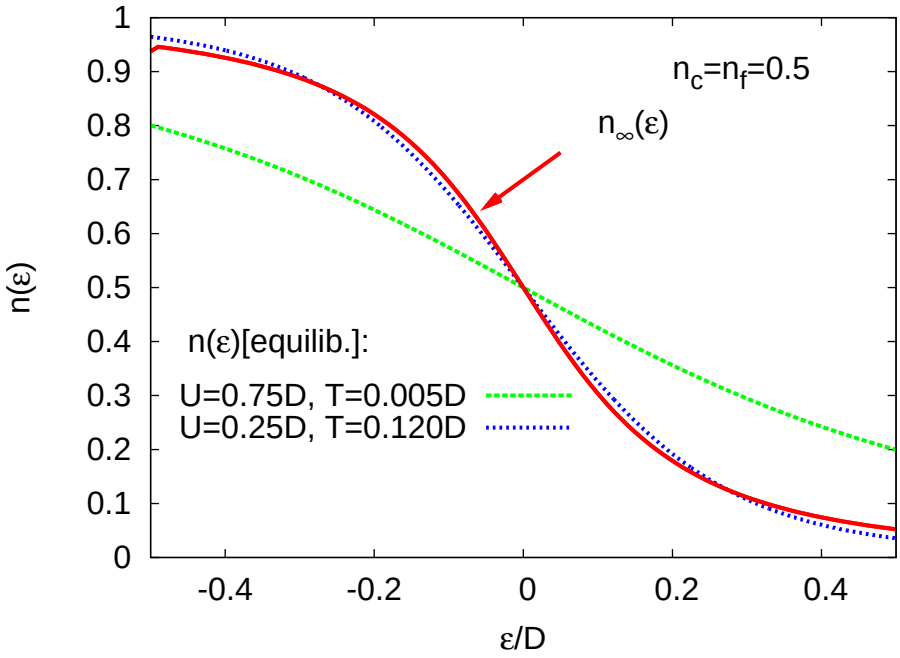

Figure 1: Occupation $n(\epsilon)$ of the single-particle eigenstates with energy ϵ for an interaction quench in the Falicov-Kimball model from $U = 0.75D$ at $t < 0$ to $U = 0.25D$ at $t > 0$ (D is the bandwidth). The initial temperature is $T = 0.005D$ (insulating state). $n_\infty(\epsilon)$ is the distribution in the stationary state after the quench, which is compared to the thermal distribution at $U = 0.25$ and $T = 0.1204D$.

infinitely long after the quench. We compare this to the distribution one would expect for a thermal state with the same particle number and total energy. The deviation clearly shows the formation of a non-thermal stationary state in this model. This behavior might be related to the immobility of one of the electron species. Thus the investigation of interaction quenches in the *Hubbard model* remains an interesting question for future research.

[1] See, e.g., J. R. Dorfman, *An Introduction to Chaos in Nonequilibrium Statistical Mechanics*, Cambridge University Press, Cambridge (1999).

[2] T. Kinoshita, T. Wenger, and D. S. Weiss, Nature **440**, 900 (2006).

[3] W. S. Fann, R. Storz, H. W. K. Tom und J. Bokor, Phys. Rev. Lett. **68**, 2834 (1992).

[4] M. Rigol, V. Dunjko, V. Yurovsky, and M. Olshanii, Phys. Rev. Lett. **98**, 050405 (2007).

[5] S. R. Manmana, S. Wessel, R. M. Noack, and A. Muramatsu, Phys. Rev. Lett. **98**, 210405 (2007).

[6] D. C. Campbell, P. Rosenau, G. M. Zaslavsky, Chaos **15**, 015101 (2005).

[7] J. K. Freericks, V. M. Turkowski, and V. Zlatić, Phys. Rev. Lett. **97**, 266408 (2006).

4 Cosimo Gorini: Transport theory beyond the Boltzmann equation – the quasiclassical approach

A standard and often convenient approach to transport problems is linear-response theory: the response of a system to an external perturbation is studied to linear order only. The advantage of this approach is that the effects of the field on the system are determined by the latter's equilibrium properties only. On the other hand, it is by definition incapable on dealing with non-linear conditions.
For quite a long while, probably the most important tool in transport theory in solids had been the much celebrated Boltzmann equation, i.e. the equation of motion for the phase-space distribution of a system, $f(\mathbf{r}, \mathbf{p}, t)$:

$$\partial_t f + \mathbf{v} \cdot \nabla_{\mathbf{r}} f + \mathbf{F} \cdot \nabla_{\mathbf{p}} f = I[f] \tag{1}$$

Reasons for its success are its ability to treat boundaries and non-linear response and its clear physical meaning. At its heart a purely classical equation, though variously improved using fenomenological arguments to be able to face some aspects of the quantum world, it shows signs of venerable age. Its fundamental shortcomings all come from its lack of microscopic foundations.
The quasiclassical approach represents a systematic way of building as general a transport theory as possible from the bottom up, ending up with the Boltzmann equation in the limit where quantum effects become negligible [1, 2]. It relies on the Keldysh formulation of non-equilibrium Green's function theory, and its central object is the Eilenberger equation, that is, the equation of motion for the $\xi-$integrated or quasiclassical Green's function, $\check{g}(\mathbf{R}, \hat{\mathbf{p}}; t, t')$. With $\xi = p^2/2m - \epsilon_F$, this is defined as

$$\check{g} \equiv \frac{i}{\pi} \int d\xi \check{G} \tag{2}$$

and, leaving aside technical considerations, it can more or less be seen as a Green's function in which small-scale details have been "washed away". Here the "check" on top of $\check{G}$ tells us that the price we pay for treating a non-equilibrium situation is a slightly more complicated structure of the Green's function, which becomes a matrix in the so-called Keldysh space:

$$\check{G} = \begin{pmatrix} G_R & G_K \\ 0 & G_A \end{pmatrix}. \tag{3}$$

G_R and G_A are the usual retarded and advanced Green's functions, with information on the spectrum of the system, while G_K is the Keldysh component, which in addition carries information on the occupation.
The quasiclassical formalism allows us to move from the microscopic Dyson equation for $\check{G}$ to the already mentioned Eilenberger equation:

$$\left[\partial_T + v_F \hat{\mathbf{p}} \cdot \partial_{\mathbf{R}}\right] \check{g}(\hat{\mathbf{p}}, \mathbf{R}; t, t') = -i \int dt_1 \left[\check{\Sigma}(\hat{\mathbf{p}}, \mathbf{R}; t, t_1), \check{g}(\hat{\mathbf{p}}, \mathbf{R}; t_1, t')\right]. \tag{4}$$

This is effectively a generalized version of the Boltzmann equation, presented here in its simplest form, able to take into account quantum interference effects to whichever order one needs to handle, for example, superconductivity or coherent spin dynamics, the latter discussed below.

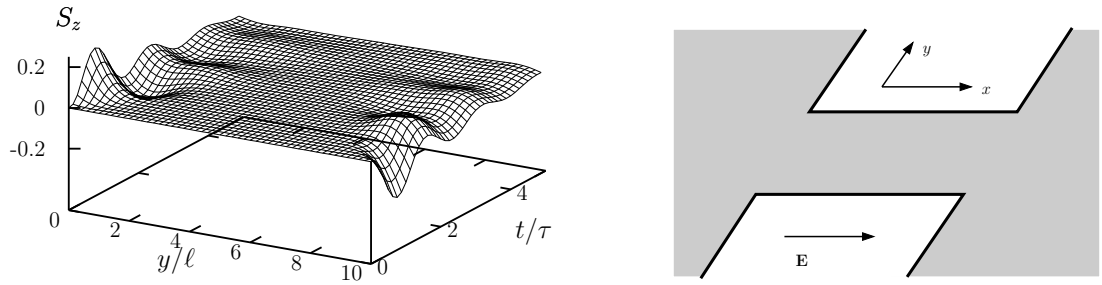

Figure 1: Left: Voltage induced spin accumulation at the edges of a 2-d electron gas, as a function of time (the voltage is turned on at $t = 0$; τ is the scattering time, l the mean free path). Right: The geometry under consideration: the grey area in the middle is the 2-d electron gas. A voltage difference along the $\mathbf{x}-$direction causes, due to spin-orbit coupling, a spin current along $\mathbf{y}$, which in turn gives rise to spin accumulation along the edges.

Applications to spin-orbit coupled, confined systems

We used the quasiclassical approach to study spin-charge coupled transport in two-dimensional electron gases, described by a Hamiltonian of the form

$$H = \frac{\mathbf{p}^2}{2m} + \mathbf{b}(\mathbf{p}) \cdot \sigma, \quad \frac{b}{\epsilon_F} \ll 1, \tag{5}$$

where $\mathbf{b}$ is an internal, spin-orbit induced, effective magnetic field. For such a system we obtained an Eilenberger equation in the form [3]:

$$\sum_{\nu=\pm} \left(\partial_T \check{g}_\nu + \frac{1}{2} \left\{ \frac{\mathbf{p}}{m} + \partial_{\mathbf{p}} (\mathbf{b} \cdot \sigma), \partial_{\mathbf{R}} \check{g}_\nu \right\} + i \left[\mathbf{b} \cdot \sigma, \check{g}_\nu \right] \right) = -i \left[\check{\Sigma}, \check{g} \right] \tag{6}$$

where ν is the band index, due to the splitting brought about in energy levels by the internal field $\mathbf{b}$. The coherence of modes lying on different bands is a crucial aspect of the problem, and also a non-trivial one. This is true especially in confined geometries, where the correct treatment of boundary conditions is of paramount importance. So far we have studied to some extent the effects of spin-charge coupling in the framework of the spin Hall effect (see Fig. 1 and [3]), and have focused on spin-relaxation in narrow wires in which different boundary conditions were assumed [4]. In the second case we were able to numerically reproduce the width-dependent behaviour of the spin-relaxation rate observed in such systems in [5]. The current effort is focused on substantially improving the boundary conditions for (6).

[1] J. Rammer, H. Smith, Rev. Mod. Phys. **58**, 323 (1986).

[2] P. Schwab, R. Raimondi, Ann. Phys. **12**, 471 (2003).

[3] R. Raimondi, C. Gorini, P. Schwab, M. Dzierzawa, Phys. Rev. B **74**, 035340 (2006).

[4] P. Schwab, M. Dzierzawa, C. Gorini, R. Raimondi, Phys. Rev. B **74**, 155316 (2006).

[5] A. W. Holleitner, V. Sih, R. C. Myers, A. C. Gossard, D. D. Awschalom, Phys. Rev. Lett. **97**, 036805 (2006).

5 Robert Hager: Kondo effect in low-carrier systems

As they are confronted with them almost every day the influence of impurities on the properties of their host material is of great interest for both experimental and theoretical physicists. Especially when magnetism comes into play the whole thing becomes even more interesting and complicated.

One specific effect induced by impurities is the Kondo effect. Although its characteristics had already been observed in the early 1930's its explanation was given only 1964 by J. Kondo [2]. The well known and often observed characteristics are a quite shallow minimum of the electrical resistance at low temperatures of the order of $10K$ together with a Curie-Weiss term in the susceptibility and a maximum of the impurity contribution to the specific heat. Materials which are typical of showing Kondo behaviour are the so called dilute magnetic alloys. This term describes non-magnetic metals which contain magnetic impurities in a relatively small concentration.

A nice example of how the resistance of a Kondo material should look like is shown in [4] although it is not the resistance but the resistivity that is plotted there. The linear decrease of the resistivity with temperature between $300K$ and about $50K$ is due to phonon scattering of the conduction electrons and completely in line with theory. For lower temperatures the phonon contribution to resistivity is predicted to decrease with T^5 and to tend to a finite value bigger than 0 for $T \to 0$. But in contrast to this prediction the resistivity reaches a minimum at $T > 0$ followed by a logarithmic increase that begins to flatten below the Kondo temperature T_K, which is approximately $T_K = 2$ in this case. After its first observation physicists did not succeed in explaining this minimum for more than 30 years.

One substantial step towards solving the problem was the observation that the existence of a resistance minimum was correlated with a Curie-Weiss term in the susceptibility which indicates the existence of local magnetic moments. Another important ingredient of Kondo's theory was the insight that interpreting the impurities as localized potential scatterers only gives a temperature independent contribution to resistivity. And as the impurities were magnetic atoms the natural thought was to take into account the impurity spin. Thus the impurities do not only act as potential scatterers but induce spin-flip scattering, too. In addition it was not enough to only treat spin-flip scattering in perturbation theory to leading order, third order terns are needed to reproduce the correct behaviour. These higher order terms contribute a term to the resistance that diverges logarithmically when $T \to 0$. For the magnetic impurities having a low concentration one can safely neglect inter-impurity interactions. What one can learn from this calculation is that the Kondo effect is a real many-particle effect caused by the interaction of impurity spin and the total spin of the conduction electrons.

In spite of the resistivity plot in [4] displaying nice Kondo behaviour it is quite unusual for the compound the data belongs to. Wigger et al. performed measurements of different properties of CaB_6 doped with U at the few atomic percent level, namely $Ca_{0.992}U_{0.008}B_6$. The reason why the presence of the Kondo effect in this material is so surprising is the following. There is another compound – LaB_6 – which is well known to show Kondo behaviour when doped with Ce at the few atomic percent level. Replacing Ce with U makes this behaviour vanish. The difference between U and Ce is that Ce has partially filled 4f-shells which are relevant for the impurity spin while U has partially filled 5f-states. These are much more broadened (in space) via hybridization with the conduction band than the Ce 4f-states and therefore lose there localized character, which is essential for the Kondo effect. Altogether one is lead to the conclusion that U impurities in non-magnetic metallic hosts do not induce Kondo physics. Nevertheless one cannot deny that $Ca_{0.992}U_{0.008}B_6$ shows quite pronounced Kondo features. To explain that the authors of [4] stress the fact that pure CaB_6 is a semiconductor and thus has

a low density of charge carriers in the conduction band. They state that thus hybridization of U 5f-states and the conduction band was less effective leading to localized impurities.

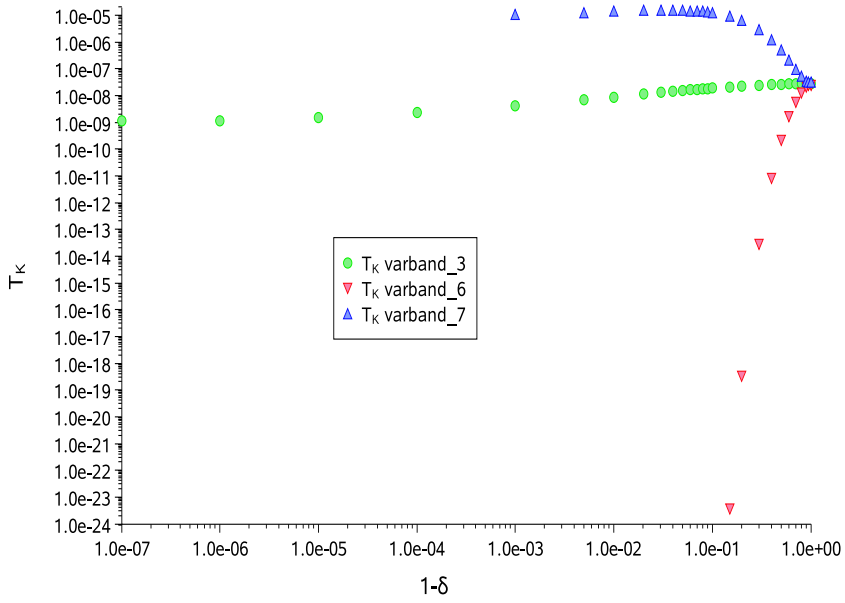

Figure 1: Kondo temperature T_K for 3 different models of the conduction band DOS (green: $\rho = \rho_0$, red: $\rho = \rho_0 \left(-|\omega - \delta|^2 + 1\right)$, blue: $\rho = \rho_0 \left(|\omega - \delta|^2 + 1\right)$) and for various fillings.

All this is a very good motivation for a theoretical simulation of the above situation. The suitable model in our case is the Single-Impurity Anderson Model (SIAM). Together with the numerical renormalization group method (NRG) we have a powerful tool to investigate the Kondo effect. The model and the method are discussed in detail by Krishna-murthy et al. [3]. For a more recent review of the NRG refer to [1]. We now investigate the following thesis. In the framework of the Anderson model strong hybridization of impurity and conduction band states leads to a high Kondo temperature. If T_K is high enough it is impossible to observe Kondo behaviour as the magnetism of the impurities is important only for low temperatures (phonon contribution to resistivity decereases with T^5). We suggest that the low carrier density in CaB_6 is responsible for an effective reduction of the hybridization strength amd thus for the lowering of the Kondo temperature. This situation is modelled via the conduction electron density of states one uses as input for the calculations. We vary the degree of filling of the conduction band from half filling to a nearly empty band described by the band shift δ going from 0 to 1. The Kondo temperature can be extracted from the impurity contribution to the entropy. This contribution drops from $ln(2)$ – contribution of a local Spin $\frac{1}{2}$ – to 0 around the Kondo temperature which is identified as the inflection point of the curve. First results with an appropriate acuracy of the entropy back up this thesis because they show obvious deviations from the predictions of the particle-hole symmetric case according to which T_K should mainly depend on the DOS at the fermi level $\rho(\omega = 0)$.

[1] Bulla, R., Pruschke, Th., und Costi, T.: cond-mat/0701105 (2007).

[2] Kondo, J.: Progress of Theoretical Physics, **32**, 37–49 (1964).

[3] Krishna-murthy, H. R., Wilkins, J. W. und Wilson, K. G.: Phys. Rev. B., **21**, 1003–1043 (1980).

[4] Wigger, G. A., Weyeneth, S., Felder, E., Ott, H. R. und Fisk, Z.: Europhys. Lett., **68**, 685–691 (2004).

6 Mamoun Hemmida: Electron Spin Resonance in Two Dimensional Magnets

The physics of low-dimensional systems such as surfaces, thin films, multilayers and low-dimensional magnets are in the focus of basic solid state research. Many of their properties are peculiarities of the reduced dimensionality of those structures. The investigation of such systems has substantially advanced our fundamental knowledge of physics, apart from the important technological applications. The study of the way in which cooperative phenomena are influenced by the dimensionality of the lattice, the symmetry of the Hamiltonian, the quantum mechanical nature of the spin, has led to such important advances as the concept of the scaling, the idea of universality and the theory of the renormalization group.
One aspect of two-dimensional (2D) systems is the topological defect. Berezinskii (1971)[3] suggested that a vortex can be some kind of topological defect. For 2D magnets Kosterlitz and Thouless (1973) [8] formulated a new theory based on a vortex-mediated phase transition of the two-dimensional XY model into a new kind of phase, the so-called topological phase. This important theory has led to an intense study of two-dimensional systems. Below a certain critical temperature, the so-called Kosterlitz-Thouless temperature $T_{KT} = \frac{\pi|J|S^2}{2k_B}$, where J is the exchange constant and S is the spin, the vortices and the antivortices are bound in vortex-antivortex pairs. Above T_{KT}, vortex-pairs unbind and start to destroy the ordered phase gradually till the magnetic system reaches the disordered phase. The temperature dependence of the correlation length $\xi(T)$, which denotes the average half distance between two free vortices, reveals an exponential divergence at T_{KT} following:

$$\xi(T) = \xi_0 \exp(b/\tau^\nu) \tag{7}$$

with $\tau = (T/T_{KT}-1)$, $\nu = 0.5$ and b=$\pi/2$. In the late 1970s, Halperin and Nelson (1978) [5] and independently Young (1979) applied the ideas of Kosterlitz and Thouless to two-dimensional crystals. They suggested that a new kind of topological defects, namely dislocation- and disclination- pairs, can mediate a melting transition and form also a topological phase. This theory suggests that the correlation length formula is similar to equation (1), with modified exponent $\nu \approx 0.37$ and without any requirement to fix the b parameter value. In the τ value T_m instead of T_{KT} denotes the melting temperature at which the dislocation-pairs start to dissociate.
In 2D magnets, the correlation length ξ can be probed by means of magnetic resonance spectroscopy, which is certainly one of the most powerful tools to investigate the magnetic properties of low-dimensional systems. One of the first observations of the Berezinskii-Kosterlitz-Thouless (BKT) phase transition in a 2D magnet was done, using nuclear magnetic resonance technique (NMR), in the honeycomb layer system $BaNi_2P_2O_8$ [4] and recently by electron spin resonance (ESR) in the isostructural compound $BaNi_2V_2O_8$. The relation between the temperature dependence of the (ESR) linewidth and correlation length, $\Delta H \sim \xi^3(T)$, was theoretically derived in [2].
Here we apply successfully the Kosterlitz-Thouless-Halperin-Nelson-Young (KTHNY) model in the two-dimensional frustrated triangular lattice antiferromagnet $LiCrO_2$ [7]. As shown in the Figure, the BKT-scenario with b=$\pi/2 \approx 1.571$ cannot give a good description of the data. Instead only a different value of b=$\pi/6 \approx 0.5236$, which does not have any theoretical justification, allows for a perfect fit. But using ν as a free fit parameter automatically yields the value $\nu \approx 0.37$ expected from the KTHNY theory. This implies some kind of fractional vortices due to spin frustration in analogy to dislocations and disclinations in a two dimensional liquid crystal.

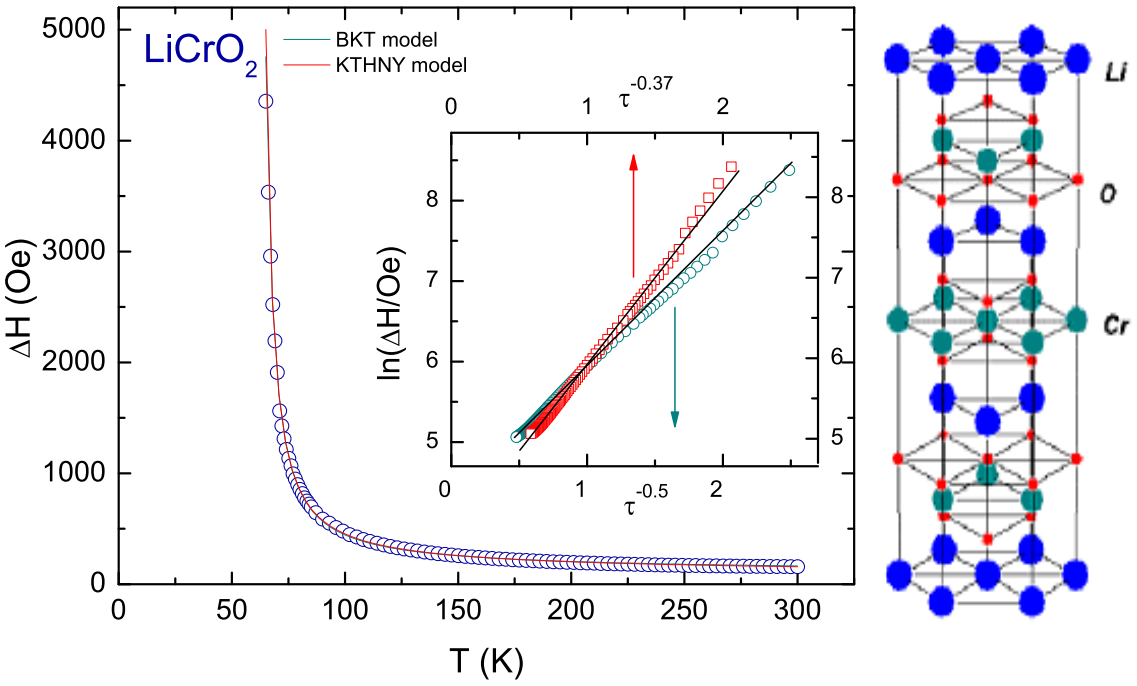

Figure 1: Left: Temperature dependence of the ESR linewidth of $LiCrO_2$ in 9.4 GHz, the inset illustrates the fit models; right: crystal structure taken from Ref. [1]

[1] L. K. Alexander et al., arXiv:cond- mat/0612435 (2006).

[2] J. Becker, PhD thesis, TU Darmstadt (1996).

[3] V. L. Berezinskii, Sov. Phys. JETP **32**, 493 (1971).

[4] P. Gaveau et al., J. Appl. Phys. **69**, 6228 (1991).

[5] B. I. Halperin and D. R. Nelson, Phys. Rev. Lett. **41**, 121 (1978).

[6] M. Heinrich et al., Phys. Rev. Lett. **91**, 137601 (2003).

[7] M. Hemmida, Master thesis, Universität Augsburg (2007).

[8] J. M. Kosterlitz and D. J. Thouless, J. Phys. C **6**, 1181 (1973).

7 Franz J. Kaiser: Coulomb repulsion effects in driven electron transport

Background

Recent experiments on the conductance of single organic molecules opened a new direction in mesoscopic transport [1]. Of particular interest is thereby the influence of electronic and vibronic excitations of the molecules which leave their fingerprints in the resulting current-voltage characteristics. Much of our knowledge about excitations of molecules is based on spectroscopy, i.e. the optical response to light. In the context of molecular conduction, it has been proposed to study as well the signatures of such excitations in the transport quantifiers like the current and its fluctuations [2]. Such experiments are at present attempted, but clearcut evidence for the proposed effects is still missing because the irradiation also causes unwanted thermal effects in the contacts, which in today's setups seem to dominate. One possibility to protect the contacts against the radiation is using the evanescent light at the tip of a near-field optical microscope.
Coupled quantum dots represent a setup with properties similar to those of molecular wires, albeit at different length and energy scales. As compared to molecular wires, they are more stable and tunable, but have the disadvantage that only a few dots can be coupled coherently. The transport properties of these "artificial molecules" can be significantly modified by microwaves [3]. It has for example been demonstrated experimentally that resonant excitations between the levels of double quantum dots result in the so-called photon-assisted transport, i.e. a significant enhancement of the dc current. A further prominent effect is adiabatic electron pumping, which is the generation of a dc current by means of a periodic variation of the conductor parameters in the absence of any net bias [4]. It has been proposed and experimentally demonstrated that pumping is more effective at internal resonances, i.e., beyond the adiabatic limit where, in addition, the pump current possesses a surprisingly low noise level [5].
Periodically time-dependent quantum systems can be described very efficiently within a Floquet theory which originally has been derived for driven closed quantum systems and later been generalised to dissipative quantum systems. Furthermore, it is possible to derive Floquet theories for the description of transport through mesoscopic conductors which are connected to external leads. For cases in which electron-electron interactions do not play any role, one can derive a Floquet scattering theory that provides exact expressions for the current and its noise. Treating the coupling between the conductor and the leads perturbatively, one can obtain a master equation for the reduced density operator of the wire. This enables a rather efficient treatment of time-dependent transport after decomposing the wire density operator into a Floquet basis. Then it is possible to study relatively large driven conductors and to include also electron-electron and electron-phonon interactions. If the time-dependent field consists of one or a few laser pulses, it is possible to obtain the density operator by propagating the Liouville-von Neumann equation.

Our work

We studied the influence of strong interaction on the transport properties of ac-driven coherent conductors. For a sketch of our sytem see Fig. 1. In particular, we compared the strongly interacting case with the opposite extreme of non-interacting electrons. Moreover, we worked out the relevance of the spin degree of freedom for weak wire-lead coupling. In our studies, we considered two archetypical effects, namely photon-assisted tunnelling through bridged molecular wires and non-adiabatic electron pumping [6].

The most significant effect is found for photon-assisted tunnelling where Coulomb repulsion renders the resonance linewidths much sharper. Thus unfortunately, interactions might contribute to the difficulties in photon-assited tunnelling experiments with molecular wires. By contrast, Coulomb repulsion is not too relevant for electron pumping in double quantum dots. For coherent current suppression, the same holds true only for parameters for which the current is already significantly reduced. Outside this region, one finds that Coulomb repulsion reduces the current essentially in the same way as in the absence of driving.
The two extreme cases of zero and very strong interaction do not necessarily allow a simple interpolation. Thus, it is desireable to extend the present studies to finite values of the interaction strength, which requires the generalisation of our formalism to at least a second excess electron. Moreover, the dc current is certainly not the only relevant quantity for the characterisation of the electron transport. Recently we studied the influence of Coulomb repulsion on, e.g., the current noise and derived therefore a master equation using Full Counting Statistics [7].

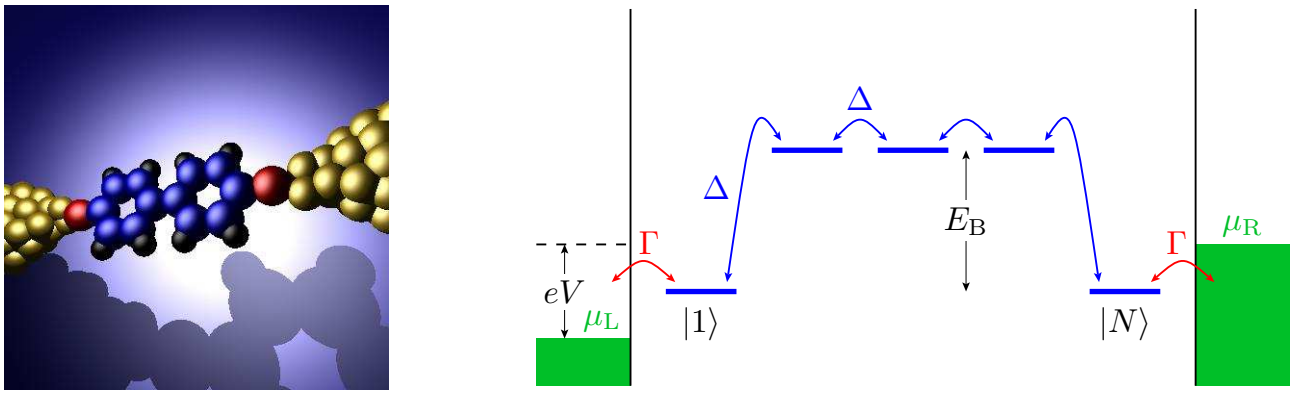

Figure 1: Sketch of a molecule with two aromatic groups between two gold electrodes (left) and a model-like level structure of such a molecule (right)

[1] J. Reichert, R. Ochs, D. Beckmann *et al.*, Driving current through single organic molecules, Phys. Rev. Lett. **88** 176804, 2002.

[2] S. Kohler, J. Lehmann and P. Hänggi, Driven transport on the nanoscale, Phys. Rep., **406** 379, 2005.

[3] W. G. van der Wiel, S. De Franceschi, J. M. Elzerman *et al.*, Electron transport through double quantum dots, Rev. Mod. Phys. **75**, 1, 2003.

[4] P. W. Brouwer, Scattering approach to parametric pumping, Phys. Rev. B **58**, 10135, 1998.

[5] M. Strass, P. Hänggi and S. Kohler, Nonadiabatic Electron Pumping: Maximal Current with Minimal Noise, Phys. Rev. Lett. **95**, 130601, 2005.

[6] F. J. Kaiser, P. Hänggi and S. Kohler, Coulomb repulsion effects in driven electron transport, Eur. Phys. J. B **54**, 201, 2006.

[7] F. J. Kaiser and S. Kohler, Shot noise in non-adiabatically driven nanoscale conductors, Ann. Phys. (Leipzig) (in press); arXiv:0705.4204

8 Rabia Kaneez: Pressure-dependent IR-UV spectroscopy on the spin-chain and spin-ladder system $(Sr,Ca)_{14}Cu_{24}O_{41}$

Infrared spectroscopy is an immense field of study of low-energy excitations in matter. The application of pressure can cause a variation of the dimensionality and phase transitions. In some materials even supercondivity is induced by applying high external pressure. These phenomena can be investigated by means of optical characterization, namely reflectivity and transmission measurements in the infrared (IR), visible (VIS), and ultraviolet(UV) frequency ranges.
The sudden interest to study ladder materials has developed due to unusual cross fertilization between theory and experiment. The motivation provided by the theorists triggered enormous efforts on the experimental front to synthesize ladder materials, searching for the two main predictions, namely the existence of a spin gap and superconductivity. Furthermore, the ladder compounds provide a playground for studies of high temperature superconductors, since in the absence of hole carriers they have a spin gap in their energy spectrum [1].
The compound $(Sr,Ca)_{14}Cu_{24}O_{41}$ is such a spin-ladder system which has been studied extensively during the last years. The crystal structure of this material consists of planes of one-dimensional CuO_2 chains and of two-leg ladders Cu_2O_3, separated by (Sr, Ca) layers (see Fig. 1). The formal Cu valency in $(Sr,Ca)_{14}Cu_{24}O_{41}$ is +2.25, i.e., hole carriers are inherently doped. Interestingly, the conductivity increases with increasing Ca content, although the total number of holes is unchanged. For low Ca content $Sr_{14-x}Ca_xCu_{24}O_{41}$ shows a semiconducting behavior, while for Ca content x=11 the material exhibits a metallic behavior along the c axis (the ladder/chain direction) down to 80 K, below which the resistivity shows an insulating behavior [2]. Most interestingly, for $(Sr,Ca)_{14}Cu_{24}O_{41}$ compounds with high Ca content superconductivity is found when external pressure is applied. The corresponding phase diagram is presented in Fig. 2. The nature of the superconductivity is unclear up to now.
$(Sr,Ca)_{14}Cu_{24}O_{41}$ is therefore an interesting material to investigate the physical properties by means of optical spectroscopy, in order to understand its normal and superconducting state. Our goal is to investigate the optical properties of $(Sr,Ca)_{14}Cu_{24}O_{41}$ single crystals by reflectivity measurements over a broad frequency range (IR to UV) under high pressure.
Our earlier pressure-dependent measurements covered the IR frequency range, which is not

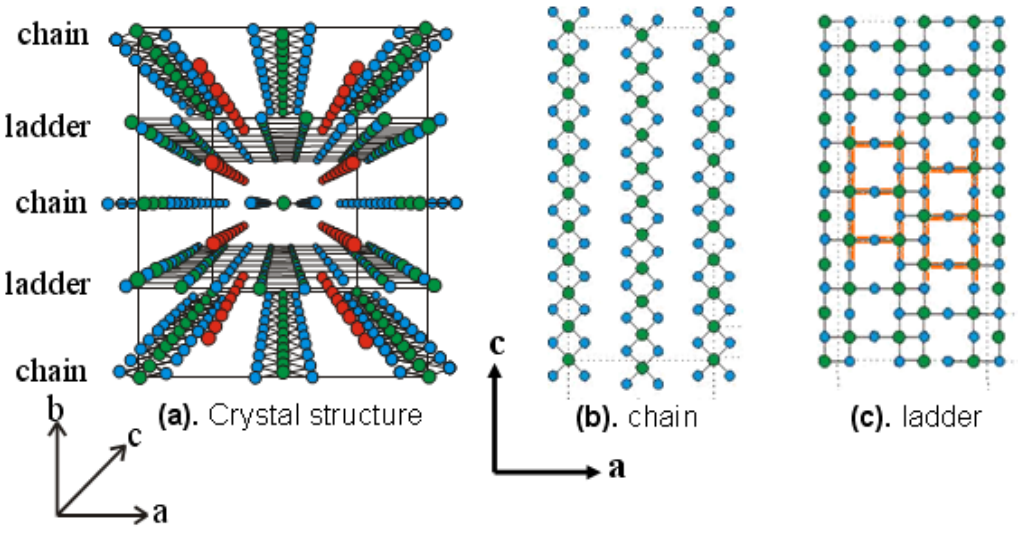

Figure 1: (a) Crystal structure of (Sr, $Ca)_{14}Cu_{24}O_{41}$; (b) and (c) show the CuO_2 chain and Cu_2O_3 ladder subunits, respectively.

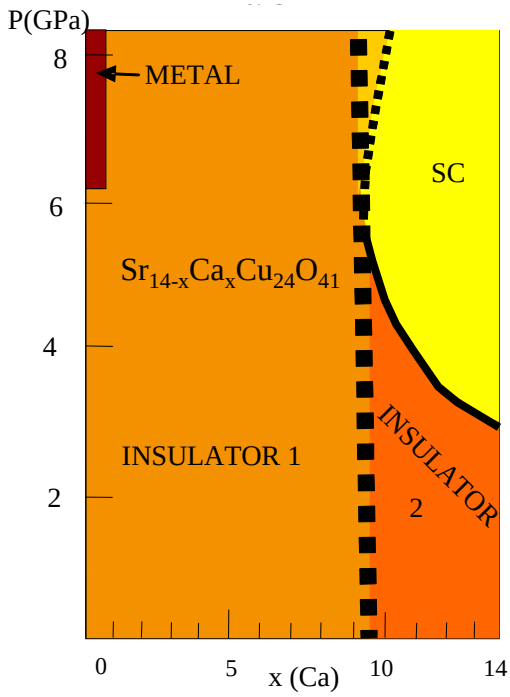

Figure 2: The phase diagram of $Sr_{14-x}Ca_xCu_{24}O_{41}$: Superconductivity is found for high Ca content under pressure.

sufficient to address specific questions like the possible redistribution of spectral weight between the VIS/UV and the IR range induced by pressure. Thus, the goal is to build up a setup for high-pressure optical investigations in the VIS and UV frequency range. Since the spectral distribution of VIS/UV light sources varies over time, it is desirable to use the double-beam technique as described in Ref. [3]. Therefore, I designed a corresponding setup which enables pressure-dependent reflection and transmission measurements in the VIS and UV frequency range at room temperature as well as at low temperature. The design of this new setup will be presented.

[1] J. G. Bednorz, and K. A. Müller, *Z. Phys. B* **64**, 188 (1986).

[2] T. Osafune, N. Motoyama, H. Eisaki, and S. Uchida, *Phys. Rev. B* **78**, 1980 (1997).

[3] K. Syassen and R. Sonnenschein, *Rev. Sci. Instrum.* **53**, 5 (1982).

9 Christian Kant, Torsten Rudolf: Infrared spectroscopy on chromium spinels

Fourier Transform Infrared (FTIR) Spectroscopy is a non-destructive experimental technique which contact-freely probes the optical conductivity of single crystals, poly crystals, liquids, gases and thin films. The sample size usually is of the order of 0.75 mm to 5 mm radius with a thickness depending on the experimental setup, which can be either transmission or reflection. With slight restrictions of the measurable frequency range a microscope adopted to the spectrometer makes it possible to investigate even much smaller samples.

The advantage of the FTIR spectroscopy is the outstanding signal-to-noise ratio, compared with the technique of dispersive spectroscopy where nearly monochromatic light is used. The real-time Fourier transformation enables the measurement of the whole frequency bandwidth of the light source which results in an instantaneous frequency-dependent reflectivity/transmittivity spectrum. Measurements can be performed in a temperature range of 3–800 K, in a broad frequency range of 20–40000 wavenumbers [cm^{-1}] (1 eV$\approx$ 8000 cm^{-1}), and in external magnetic fields of up to 7 T. Due to varying optical properties of cryostat windows, reference mirrors and detectors, one carefully has to choose the correct setup in the considered frequency range. Thereby one has to distinguish between the
i) far infrared (20–700 cm^{-1}), where the energies of the optical phonon modes of solid states and vibrational and rotational modes of gaseous molecules are located,
ii) the mid infrared (700–8000 cm^{-1}), where vibrations of covalent bound gaseous molecules and group frequencies of organic functional groups can be detected, as well as band gaps, polarons and electronic (intraband and interband) transitions which also can be found at higher energies, namely the
iii) near infrared (8000–14000 cm^{-1}), the
iv) region of visible light (14000–26000 cm^{-1}), and the
v) ultraviolet range (26000–40000 cm^{-1}).

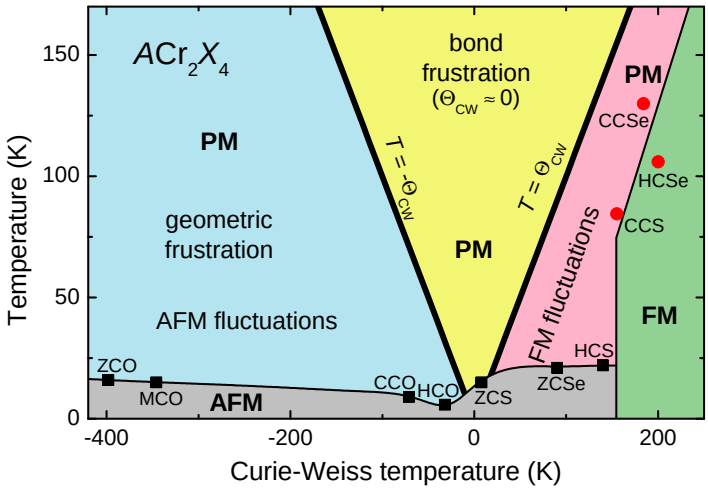

Figure 1: Schematic magnetic phase diagram of ACr_2X_4 compounds, where characteristic temperatures are plotted versus the Curie-Weiss temperature. Hypothetical magnetic ordering temperatures ($T = \pm\Theta_{CW}$) are indicated by thick solid lines. The distance between the thick line and the actual magnetic ordering temperature is a direct measure of the frustration in the system. [1]

The success of FTIR spectroscopy begun with the invention of fast microprocessors about 50

years ago and thanks to its versatile physical utility it is not astonishing that this technique is nowadays often used in chemical, preparative and analytical research and industry.

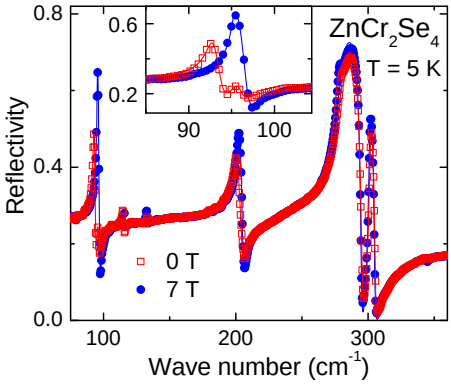

Figure 2: Typical reflectivity spectra of $ZnCr_2Se_4$ at 5 K. On can clearly see the four IR active phonon modes. The splitting of the mode close to 100 cm^{-1} below the antiferromagnetic phase transition can be suppressed by an external magnetic field (see inset), which indicates a spin-driven Jahn-Teller effect being responsible for the phonon splitting. [2]

The basic condition for the visibility of lattice oscillations in the far infrared is the existence of a static dipole moment or a dipole moment which can be excited by the incoming electromagnetic wave. A complementary technique is the Raman Spectroscopy, where not the dipole moments can be detected, but polarizabilities of molecules changed by the incident light. Group theory can theoretically predict the number of IR and Raman active modes of a solid state by taking into account the symmetry space group and the actual ("Wyckoff") positions of the ions.

This talk gives basic information about the experimental setup of the FTIR spectrometer, the measured quantities, some theory which is necessary to understand how physical quantities are derived, such as transverse ω_{TO} and longitudinal optical ω_{LO} frequency of a phonon mode, its damping γ and strength $\Delta\epsilon$, dielectric permittivity ϵ', dielectric loss ϵ'', complex optical conductivity $\sigma^* = \sigma' + i\sigma''$, plasma frequencies Ω_p, effective charges Ze, etc.
Additionally results of reflectivity measurements on chromium spinels ACr_2X_4 are shown with the magnetic Cr ion located at the B site, A =Zn, Cd, Hg, and X =O, S, Se. Exemplarily various physical effects like spin-phonon coupling, geometric and bond frustration due to competing ferromagnetic and antiferromagnetic exchange interactions, and a spin-driven Jahn-Teller effect are introduced and explained. [1, 2, 3]

For further information on Fourier Transform Infrared Spectroscopy please see reference [4].

[1] T. Rudolf, Ch. Kant, F. Mayr, J. Hemberger, V. Tsurkan, and A. Loidl, New J. Phys. **9**, 76 (2007).

[2] T. Rudolf, Ch. Kant, F. Mayr, J. Hemberger, V. Tsurkan, and A. Loidl, Phys. Rev. B **75**, 052410 (2007).

[3] J. Hemberger, T. Rudolf, H.-A. Krug von Nidda, F. Mayr, A. Pimenov, V. Tsurkan, and A. Loidl, Phys. Rev. Lett. **97**, 087204 (2006).

[4] P. R. Griffiths, J. A. de Haseth, *Fourier Transform Infrared Spectrometry*, Wiley Interscience, New York, Chichester, Brisbane, Toronto, Singapore (1986).

10 Michael Krispin: Preparation and characterization of Fe- and Co-oxide nanoparticles

Nanosized transition metal oxides particles can be expected to show size dependent optical, magnetic and chemical properties with possible applications in catalysis, magnetic and optical devices. The size dependence of physical properties can be associated with an influence of particle dimension on the electronic structure of the material. It has already been shown, that catalytic and magnetic properties of nanoparticles might be quite different from bulk materials. An example are nanosized particles of the compound Fe_2O_3, which exhibit superparamagnetism. [1]
The electronic structure of nanosized iron oxide has been investigated by scanning probe microscopy (SPM) and spectroscopy (STS) as well as by photoelectron spectroscopy (PES) and optical spectroscopy. Extended X-ray absorption fine structure (EXAFS) measurements were carried out to probe the local crystal structure of the nanoparticles. To produce nanosized iron oxide particles we utilized the ability of ferritin to self-assemble and construct a core of iron oxide. Ferritin is the major cellular iron-storage protein and consists of a spherical hollow shell. The inner and outer diameters of the protein shell are about 8 and 12.5 nm, respectively. The iron core shows a structure similar to that of the mineral ferrihydrite ($5\ Fe_2O_3 \cdot 9\ H_2O$). [2] Channels penetrate the protein shell and provide the means by which iron and other atoms can be accumulated within or removed from the molecules. In previous work, ferritin was used to prepare several kinds of nanoparticles. [3, 4] Protein shell and water were removed by oxidation in air. This preparation process resulted in a nanoparticle diameter of ~ 6 nm for the native ferritin precursor and ~ 3.5 nm for the remineralized ferritin precursor respectively. Figure 1 shows atomic force microscopy (AFM) pictures of monolayers of the annealed particles.

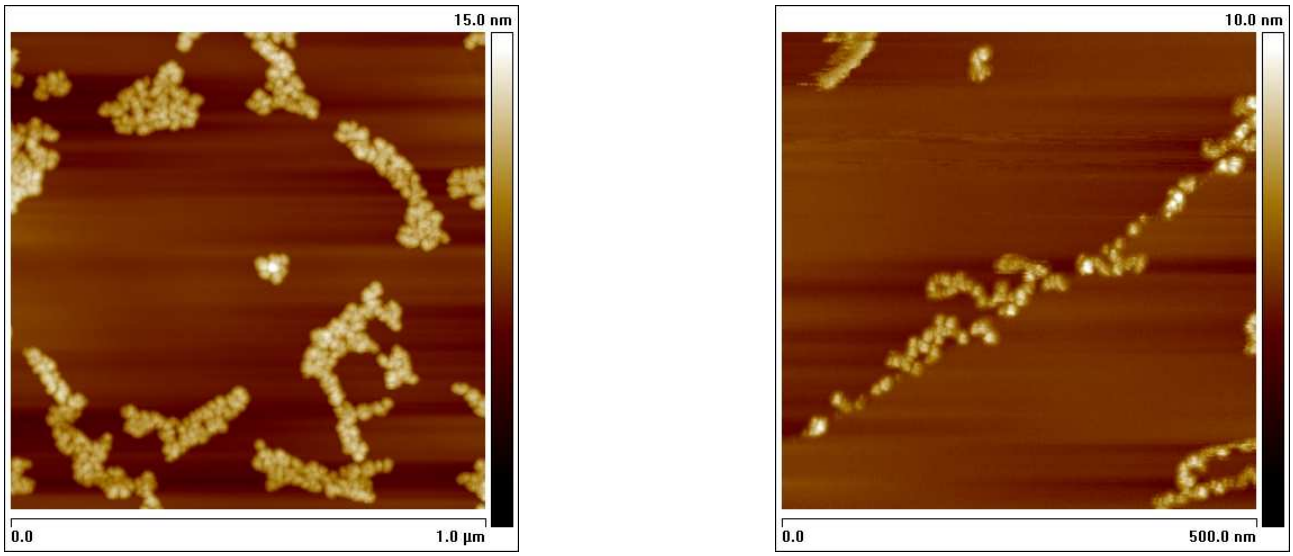

(a) native ferritin (b) remineralized ferritin

Figure 1: AFM images of native (left) and remineralized ferritin molecules (right) after annealing

Depending on the annealing parameters, we obtain nanoparticles of different iron oxide phases for the 6 nm particles. X-ray diffraction and transmission electron microscopy revealed γ-Fe_2O_3, α-Fe_2O_3, and a intermediate phase of both [5]. PES measurements on these nanoparticle phases show spectra characteristic of Fe_2O_3 corresponding to a Fe^{3+} state.

To investigate the electronic structure of single nanoparticles we performed STS measurements on the different phases of the 6 nm particles. Only nanoparticles of the thermodynamically stable α-Fe_2O_3 phase show a band gap of 2.0 eV compatible to the bulk material. [5] The STS measurements on all other nanoparticle phases demonstrate the existence of a surface band gap of 1.3 eV, although volume-sensitve optical spectroscopy reveal a band gap corresponding with the bulk material.

The local crystal structure of the iron-oxide nanoparticles was investigated by EXAFS measurements at the iron K-edge. Spectra of the 6 nm particles with high particle density (particles per volume)(A) and low density (B), 3.5 nm particles (C) and a nanopowder α-Fe_2O_3 reference can be seen in Fig. 2. The spectra can be fitted with a α-Fe_2O_3 model using lattice parameters and atomic positions from a bulk sample. [6] In comparison to the structural input of the bulk hematite model, the fit to the α-Fe_2O_3 reference sample shows a slight decrease of the nearest neighbor Fe–O distance R (i.e. within the iron-oxygen octahedron) of 0.02 Å. This distance decreases further for the nanoparticle samples A – C as can be seen in Fig. 3. This change in bond length is attributed to the formation of iron sites of tetrahedral coordination near the surface of the nanoparticles. Based on this observation a core–shell model is suggested for the nanoparticles with a tetrahedral coordinated shell and a α-phase like core.

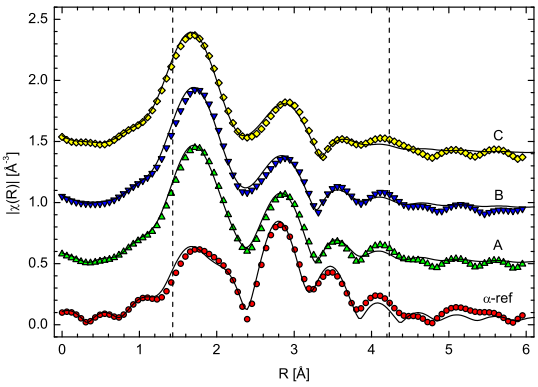

Figure 2: FT-EXAFS spectra (symbols) of α-Fe_2O_3 reference and samples A – C and according fits with the α-Fe_2O_3 model (solid lines)

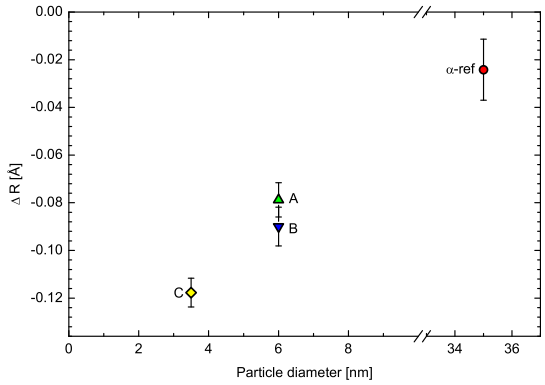

Figure 3: Change of the Fe–O bond length within the fist shell in comparison to the α-Fe_2O_3 model. [6]

[1] C. Janzen, J. Knipping, B. Rellinghaus, P. Roth, *J. Nanop. Res.* 5 (2003), p. 589.

[2] S. Mann, J. Webb, R. J. P. Williams, Biomineralization, VCH, Weinheim (1989).

[3] K. K. W. Wong, S. Mann, *Adv. Mater.* 8 (1996), p. 928.

[4] H. A. Hosein, D. R. Strongin, M. Allen, T. Douglas, *Langmuir* 20 (2004), p. 10283.

[5] M. Preisinger, M. Krispin, T. Rudolf, S. Horn, D. R. Strongin, *Phys. Rev. B* 71 (2005), p. 165409.

[6] H. Sawada, *Mat. Res. Bull.* 31 (1996), p. 141.

11 Stephan Krohns: Colossal dielectric constants and multiferroic behaviour

Dielectric spectroscopy allows to measure in a broad frequency range ($10^{-6} - 10^{15}$ Hz) by using a variety of different measurement devices and techniques. It includes time domain measurements, frequency response analysis, autobalance bridge, reflection and transmission techniques, resonance and quasi-optic measurements and finally optical spectroscopy. All these methods allow to gain information about the dielectric properties of a material, determined, e.g., by dipolar, ionic and electronic polarisation contributions.

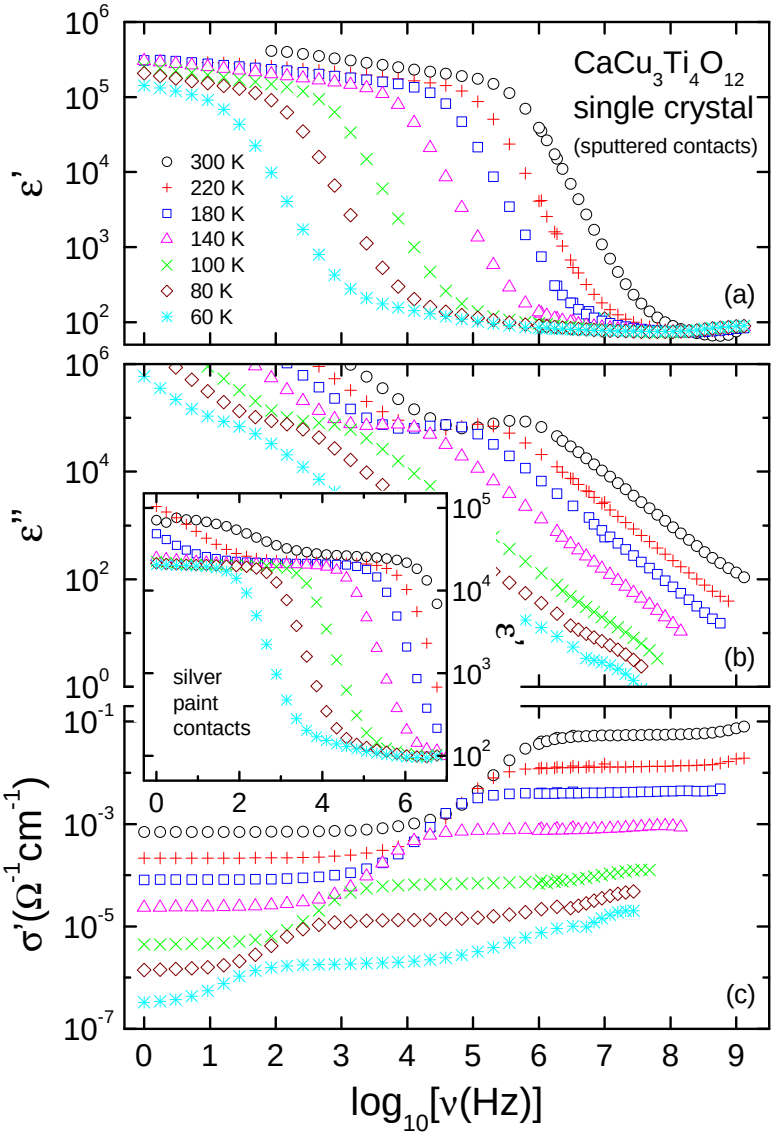

Figure 1: Frequency-dependent dielectric constant (a), loss (b), and conductivity (c) of single-crystalline CCTO with sputtered gold contacts at various temperatures. The inset shows ϵ' for the same sample using silver paint contacts. [1]

Aside of purely academic interest, the complete frequency range from Hz to GHz and especially the high frequency range, is as well of high relevance for applications of dielectrics, e.g., in

integrated circuits and microelectronic devices. Within the SFB-project E4, amongst others, the origin of colossal dielectric constant (CDC) and multiferroic behaviour of various materials are investigated.
One prominent representative of CDC materials is $CaCu_3Ti_4O_{12}$ (CCTO) [2], which shows an extremely high dielectric constant (up to $\epsilon' \approx 10^6$) in a broad frequency and temperature range (see figure 1). Possible intrinsic origins of this outstanding dielectric behaviour could be, e.g., ferroelectricity (ionic or electronic), relaxation of defects or charge density waves. There was a lot of research in the past six years aiming at clarifying the origin of the colossal dielectric constant in CCTO. It soon became clear that the colossal ϵ' must have a non-intrinsic origin, which can be explained by a Maxwell-Wagner relaxation [3]. There seems to be some consensus in the community that this extrinsic effect is related to „internal barrier layer capacitors“ (IBLC), but the results of dielectric spectroscopy of polycrystalline samples and of a CCTO single crystal presented in this talk, reveal strong evidence for a „surface barrier layer capacitor“ (SBLC) model, which can be realized, e.g., by a Schottky diode. To verify this statement lots of measurements were done using different metal contacts, polishing sample surface under different atmospheres (air and nitrogen) and grinding the surface to modify its roughness. A further very interesting finding is the occurrence of a strong second dispersion, related to much higher absolute values of dielectric constant, not only in polycrystalline samples but also in single crystals (see inset of figure 1). This second relaxation can be influenced by surface variation, too.

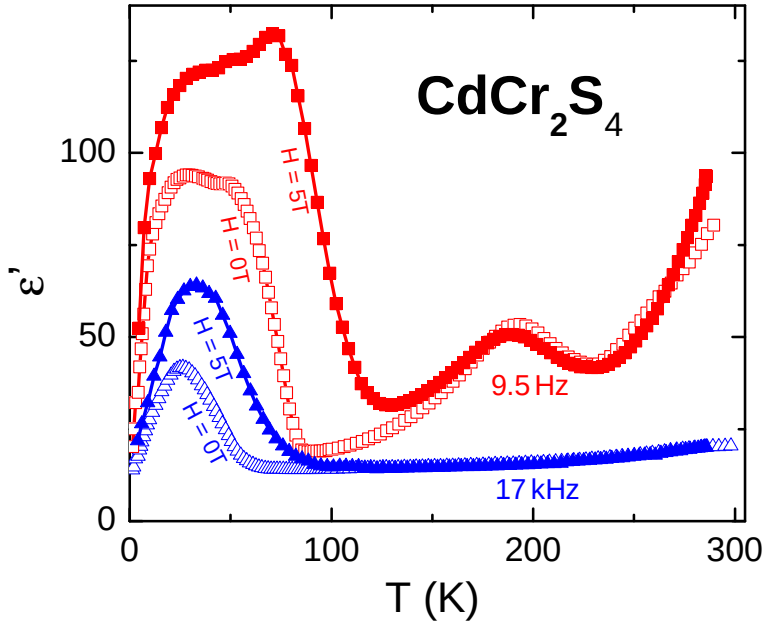

Figure 2: Dielectric constant versus temperature at 9.5 Hz and 17 KHz, measured at zero field and in an external magnetic field of 5 T, directed perpendicular to the electric field. [4]

Besides the well-known multiferroic rare-earth manganites, a new class of materials, Cr based spinels, show multiferroic behaviour, too. A prominent representative of this class is $CdCr_2S_4$ (CCS) (see figure 2), where ferromagnetism and proper ferroelectricity coexist and colossal magnetocapacitive effects and strong coupling of ferroelectric polarisation to external magnetic

fields are found [4]. While the magnetic ordering is well understood in the framework of electronic superexchange, the ferroelectric properties are still controversially discussed. Especially the origin of the detected this relaxor behaviour may be doubted and ascribed to a conductive artefact. In the second part of the talk this notion will be discussed and new experiments will be presented. [5]

[1] S. Krohns, P. Lunkenheimer, S.G. Ebbinghaus, and A. Loidl, cond-mat/0612569.

[2] C.C. Homes, T. Vogt, S.M. Shapiro, S. Wakimoto, and A.P. Ramirez, Science **293**, 673 (2001).

[3] P. Lunkenheimer, R. Fichtl, S.G. Ebbinghaus, and A. Loidl, Phys. Rev. B **70**, 172102 (2004). T.B. Adams, D.C. Sinclair, and A.R. West, Phys. Rev. B **73**, 094124 (2006).

[4] J. Hemberger, P. Lunkenheimer, R. Fichtl, H.-A. Krug von Nidda, V. Tsurkan, A. Loidl, Nature **434**, 364 (2005).

[5] J. Hemberger, P. Lunkenheimer, R. Fichtl, H.-A. Krug von Nidda, V. Tsurkan, A. Loidl, Nature brief communication, unpublished. G. Catalan and J.F. Scott, cond-mat/0607500. P. Lunkenheimer, J. Hemberger, V. Tsurkan, D. Staresinic, K. Biljakovic, and A. Loidl, cond-mat/0701417.

12 Hyun-Jung Lee: Numerical Renormalization Group Calculations for Impurity Quantum Phase Transitions

The NRG, originally developed for the solution of the Kondo problem, proved the power of a non-perturbative method in other impurity models by successfully describing the physics of quantum phase transitions and quantum critical points of the models. At the begining of the talk, we introduce general concepts of quantum phase transition and address the relevant physical questions of the impurity models. After discussing the technical details of the NRG, we present our recent results on the two impurity models, the spin-boson model and the bosonic single-impurity model.

The quantum phase transition of the spin-boson model [1] has a long history but most of achievements were reached for the ohmic dissipation. In the ohmic case, a delocalized and a localized phase are separated by a Kosterlitz-Thouless transition at the critical coupling $\alpha = 1$. The new development of the NRG treating the bosonic degrees of freedom broadened the range of the parameter space to include the sub-ohmic case and, as a result, we found second order transitions dividing the parameter space into the localized and the delocalized phases, where the two-level system stays either at the two-fold degenerate eigenstates of $\hat{\sigma}_z$ (localized) or the single lowest eigenstate of $\hat{\sigma}_x$ (delocalized). The two-fold degeneracy in the localized phase and the lifting in the delocalized phase are manifested in the residual value of S_{imp} by the $\ln 2$ difference. In the quantum critical phase, the residual entropy is quenched to a value be-

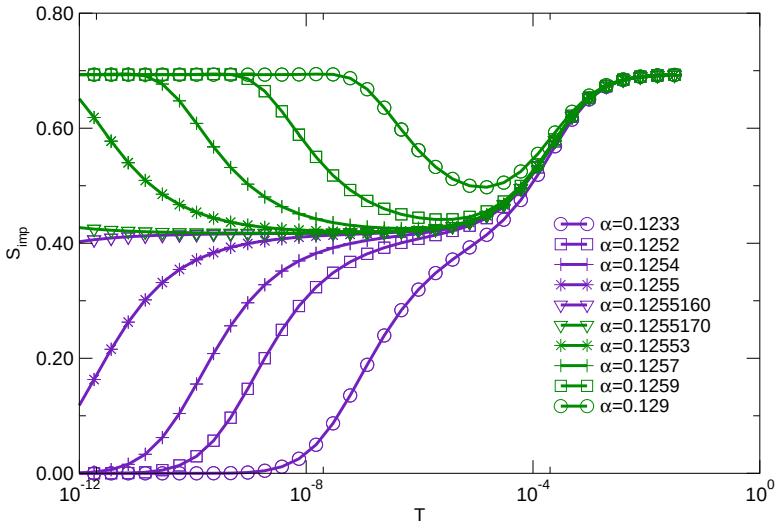

Figure 1: Temperature dependence of the impurity contribution to the entropy, $S_{imp}(T)$, in the sub-ohmic case ($s = 0.8$) for various values of α.

tween 0 and $\ln 2$, implying that the subsystem is fluctuating for arbitrarily small temperature T (Fig. 1). The origin of the quantum fluctuation could be clarified with analysing the structure of the quantum critical fixed points. We expect that, in the vicinity of the critical dimensions $s = 0$ and $s = 1$, the many-particle spectrum at the quantum critical points is perturbatively

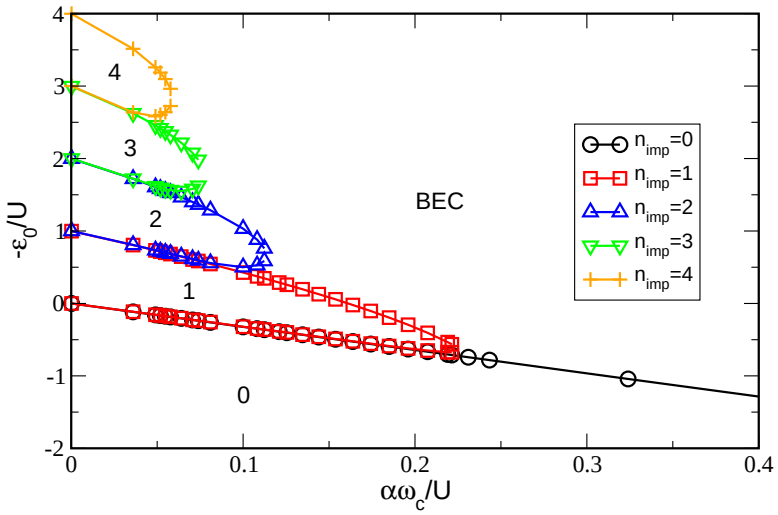

Figure 2: Zero-temperature phase diagram of the bosonic siAm for bath exponent $s = 0.6$ and fixed impurity Coulomb interaction $U = 0.5$. The different symbols denote the phase boundaries between Mott phases and the BEC phase. The Mott phases are labeled by their occupation n_{imp} for $\alpha = 0$. Only the Mott phases with $n_{imp} \leq 4$ are shown. The NRG parameters are $\Lambda = 2.0$, $N_b = 10$, and $N_s = 100$.

accessible within a single-particle picture [2] [3] [4].

A model with a bosonic impurity state coupled to a non-interacting bosonic surrounding, what is called, the bosonic single-impurity Anderson model, is studied with the NRG to show that there exist quantum phase transitions and quantum critical points separating the BEC (Bose-Einstein condensation) phase from the Mott phases (Fig. 2). The BEC phase corresponds to a macroscopic occupation of a localized state around the impurity. In the Mott phase, the local Coulomb repulsion prevents Bose-Einstein condensation. One of our motivation for studying the bosonic single-impurity Anderson model comes from a treatment of the Bose-Hubbard model within dynamical mean-field theory (DMFT), for which we calculate the dynamical quantities of the impurity model, such as impurity spectral function and self-energy, to make a self-consistent connection to the lattice system [5].

[1] A. J. Leggett, S. Chakravarty, A. T. Dorsey, M. P. A. Fisher, A. Garg, and W. Zwerger, Rev. Mod. Phys. **59**, 1 (1987).

[2] R. Bulla, N.-H. Tong and M. Vojta, Phys. Rev. Lett. **91**, 170601 (2003).

[3] R. Bulla, H.-J. Lee, N.-H. Tong and M. Vojta, Phys. Rev. B. **71**, 045122 (2005).

[4] H.-J. Lee, R. Bulla and M. Vojta, J. Phys.: Condens. Matter. **17**, 6935 (2005).

[5] H.-J. Lee and R. Bulla, Eur. Phys. J. B **56**, 199 (2007).

13 Günter Obermeier: Metal–insulator transition of V_2O_3 thin films investigated by surface acoustic waves

Stoichiometric V_2O_3 exhibits a metal–insulator (MI) transition upon cooling at around $T_{MI} = 160\ K$ with a hysteresis of about $10\ K$ upon thermal cycling (see [1, 2] and references therein). The transition is accompanied by magnetic ordering (paramagnetic to antiferromagnetic) and by a lowering of lattice symmetry (trigonal to monoclinic) reducing the volume by 1.4%.
Although V_2O_3 has been studied extensively over several decades, the interplay between lattice as well as magnetic and electronic degrees of freedom has not been completely understood. Often the importance of electronic correlations is emphasized and the semiconducting phase is regarded as a Mott insulator [2, 3]. But also the influence of the electron-phonon interaction has to be taken into account [4].
In single crystals the formation of microcracks induced by the volume change through the transition makes it nearly impossible to investigate the elastic properties of V_2O_3. Therefore measurements of the elastic constants are rare, but could contribute valuable information concerning the coupling of electronic and lattice degrees of freedom.
Thin films of V_2O_3 are not destroyed on passing the MI transition. The pinning of the film to the substrate provides a preferred orientation for the structural distortion, so that all domains which build up at the transition are distorted in the same direction, thus reducing the internal stress. Additionally, stress is also released at the grain boundaries of the (textured) films.
Surface acoustic waves (SAW), generated at and propagating along the surface of a piezoelectric material, are an ideal tool to investigate the MI transition of such thin films with respect to their electronic and elastic properties.

Thin V_2O_3 films of thicknesses of around $d = 400\ nm$ were grown in an UHV chamber by electron beam evaporation from a V_2O_3 polycristalline target onto piezoelectric $LiNbO_3$ substrates, followed by annealing treatments under reducing atmosphere. The films were characterized by AFM, XRD and electrical resistivity measurements. The temperature dependence of the sound velocity and the attenuation of the SAW was measured utilizing interdigital transducers, i. e. microstructured finger electrodes made of aluminum placed on the substrate.

The measured electrical resistance and the sheet conductance, respectively, shown in fig. 1 a) change by at least six orders of magnitude. The lower transition temperature T_{MI} compared to stoichiometric bulk material can be explained by internal strain, as inferred from XRD.
Based on theories about piezoelectrica covered with semiconducting [5] and conducting films [6] equations were obtained to describe the interaction of the SAW with the V_2O_3 layer regarding the measured attenuation (fig. 1 b) and the measured shift of the sound velocity (curve A in fig. 1 d). The calculated values of the attenuation (fig. 1 c) and of the sound velocity shift (curve AT in fig. 1 d) do not cover the whole temperature range because the calculations use the sheet conductance as input which could only be measured to a limited extent.
While the measured and calculated temperatures of the attenuation maxima coincide, the shape of the maxima is only in qualitative agreement. Similar situation for the velocity: while the step height of curve A after subtraction of the additional contribution labeled QF (discussed below) equals the calculated height (curve AT), the increase of the sound velocity with decreasing temperature is smoother than calculated. These differences could probably arise from a high relative permittivity of V_2O_3, whereas the models used for calculation neglect this influence.
The decrease of the sound velocity shift beginning already $60\ K$ above T_{MI} (QF) indicates a softening that cannot be explained by simple electrical models. This behavior may be regarded as a precursor of the MI transition.

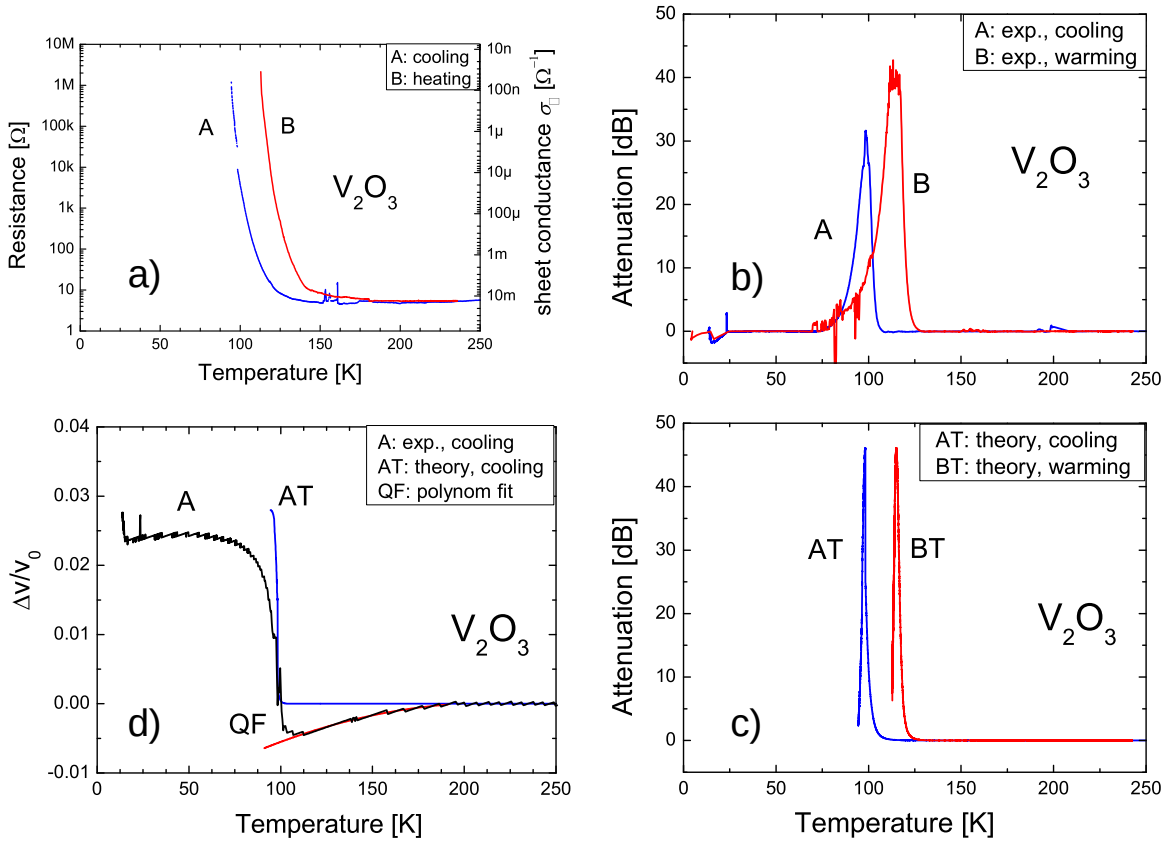

Figure 1: Temperature dependence of a) the electrical resistance and sheet conductance of a V_2O_3 film, b) the measured attenuation of the SAW compared to c) calculated values, and d) the velocity shift of the SAW measured upon cooling (labeled A) compared to calculated values (labeled AT). The calculations are based on refs. [5, 6], see text. The plots above were compiled from ref. [7].

To distinguish between signals arising from the electrical and the elastic part of the SAW there is currently work in progress to produce films with metallic interlayers to short circuit and therefore suppress the electrical contribution of the SAW and thus separate only the elastic properties.

[1] W. Brückner, H. Oppermann, W. Reichelt, J. I. Terukow, F. A. Tschudnowski, and E. Wolf, *Vanadiumoxide*, Akademie, Berlin, (1983).

[2] M. Imada, A. Fujimori, and Y. Tokura, Rev. Mod. Phys. **70**, 1039 (1998).

[3] K. Held, G. Keller, V. Eyert, D. Vollhardt, and V. I. Anisimov, Phys. Rev. Lett. **86**, 5345 (2001).

[4] M. Yethiraj, S. A. Werner, W. B. Yelon, J. M. Honig, Phys. Rev. B **36**, 8675 (1987).

[5] K. A. Ingebrigtsen, J. Appl. Phys. **41**, 454 (1970).

[6] A. R. Hutson and D. L. White, J. Appl. Phys. **33**, 40 (1962).

[7] C. Müller, A. A. Nateprov, G. Obermeier, M. Klemm, R. Tidecks, A. Wixforth, and S. Horn, J. Appl. Phys. **98**, 084111 (2005).

14 Alexej Pashkin, Helge Hoffmann: Pressure dependence of the low-dimensional compounds TiOCl and TiOBr

TiOCl and TiOBr are low-dimensional compounds whose orthorhombic (Pmmn) crystal structures consist of Ti-O bilayers within the ab plane separated by Cl/Br ions [1, 2]. As an example, the crystal structure of TiOCl is shown in Fig. 1. TiOCl and TiOBr raised a lot of interest recently, since they are spin-Peierls systems with puzzling properties [3, 4, 5, 6]: Two successive phase transitions occur [3]; the transition at T_{c2} (91 K in TiOCl and 48 K in TiOBr) is a transition to an incommensurate spin-Peierls state, followed by a lock-in transition to a commensurate dimerized state below T_{c1} (67 K in TiOCl and 27 K in TiOBr).

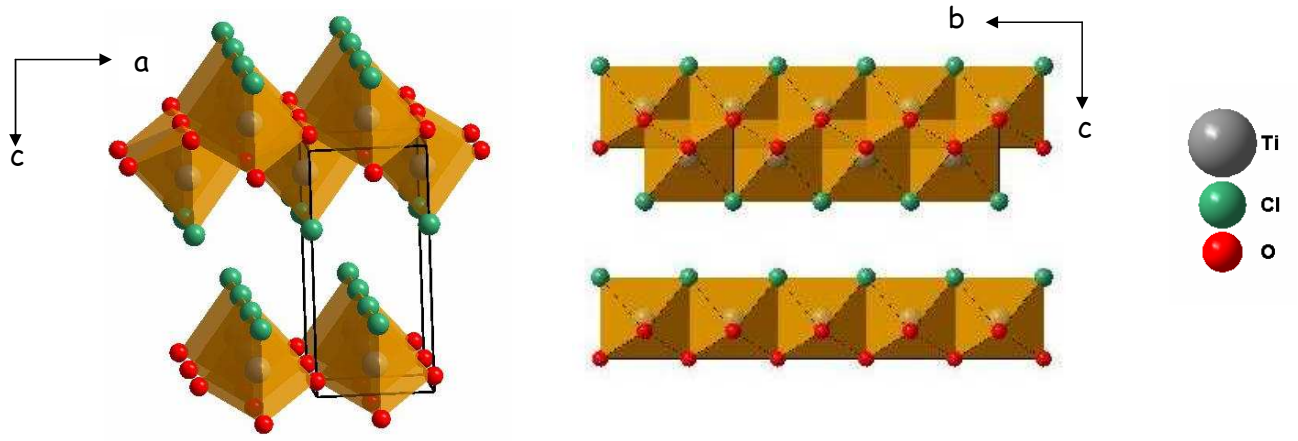

Figure 1: Crystal structure of TiOCl: Ti-O bilayers within the ab plane are separated by Cl ions.

Regarding the electronic properties, TiOCl and TiOBr are Mott-Hubbard insulators with a charge gap of about 2 eV. We recently carried out room-temperature optical measurements on TiOCl as a function of external pressure over a broad frequency range (infrared to visible) and found indications for an insulator-to-metal transition at around 12 GPa (using CsI as pressure transmitting medium) [7]: namely a strong suppression of the transmittance and an abrupt increase of the reflectance. In Fig. 2 the pressure-dependent transmittance and absorbance spectra are presented, as well as the measurement geometries. In TiOBr similar pressure-induced effects are observed [8].
Presently, it is unclear whether the observed insulator-to-metal transition in TiOCl and TiOBr is due to a pressure-induced tuning of the bandwidth (bandwidth-controlled Mott transition) or due to a structural phase transition under pressure. We therefore carried out pressure-dependent x-ray diffraction studies under pressure to obtain information about the changes of the crystal structure close to the pressure-induced insulator-to-metal transition in TiOCl and TiOBr. The measurements on the powder samples were carried out at beamline ID09A of the ESRF in Grenoble. For pressure generation diamond anvil pressure cells were used, which allowed to cover a wide pressure range (up to pressures above 20 GPa). The results and their interpretation will be presented.

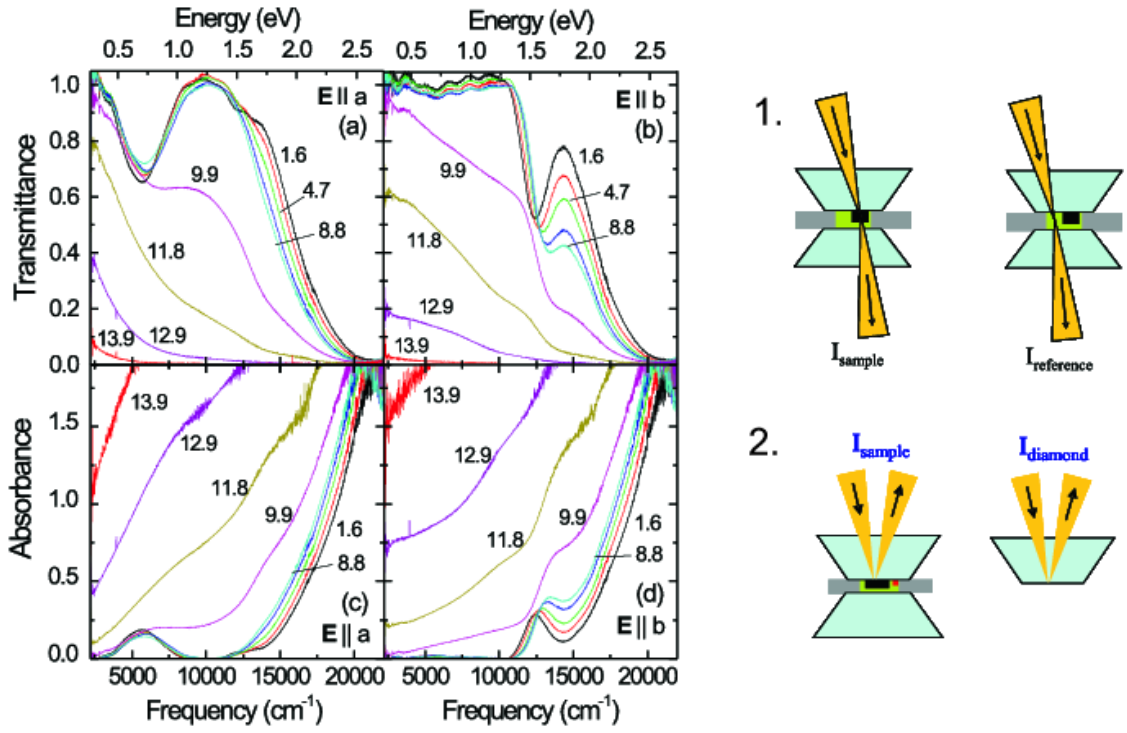

Figure 2: Left: Transmittance and absorbance spectra of TiOCl as a function of pressure for the polarizations $E||a$ and $E||b$ [7]. Right: Transmission (1.) and reflection (2.) geometry for high pressure measurements.

[1] H. Schäfer, F. Wartenpfuhl und E. Weise, *Zeitschrift f. anorganische und allgemeine Chemie* **295**, 267 (1958).

[2] H. G. v. Schnering, M. Collin und M. Hassheider, *Zeitschrift f. anorganische und allgemeine Chemie* **387**, 137 (1972).

[3] A. Seidel, C. A. Marianetti, F. C. Chou, B. Ceder, and P. A. Lee, *Phys. Rev. B* **67**, 020405 (2003).

[4] M. Shaz, S. van Smaalen, L. Palatinus, M. Hoinkis, M. Klemm, S. Horn, and R. Claessen, *Phys. Rev. B* **71**, 100405 (2005).

[5] S. van Smaalen, L. Palatinus, and A. Schönleber, *Phys. Rev. B* **72**, 020105 (2005).

[6] A. Krimmel, J. Strempfer, B. Bohnenbuck, B. Keimer, M. Hoinkis, M. Klemm, S. Horn, A. Loidl, M. Sing, R. Claessen, and M. v. Zimmermann, *Phys. Rev. B* **73**, 172413 (2006).

[7] C. A. Kuntscher, S. Frank, A. Pashkin, M. Hoinkins, M. Klemm, M. Sing, S. Horn, and R. Claessen, *Phys. Rev. B* **74**, 184402 (2006).

[8] C. A. Kuntscher et al., to be published.

15 Stefan Riegg: Magnetic and Electrical Transitions in La_2RuO_5

Various lanthanum ruthenates possess perovskite type stuctures, or layered stuctures, which can be derived from the ideal perovskite [1], like the Ruddlesden-Popper- and the [110]-phases. La_2RuO_5 can be considered a member of the [110]-group. It possesses a layered structure (see Fig. 1) consisting of RuO_6 octahedra and La-ions alternating with LaO_2 plains.
Crystal structure analysis has been done by Rietveld-Refinement of X-ray powder, neutron and synchrotron radiation diffraction data [2], [3]. Measurements at different temperatures show that a stuctural transition occurs in a broad range between 160 K and 190 K. The monoclinic high-temperature phase (ht: Space group $P2_1/c$) changes to a triclinic low-temperature phase (lt: $P\bar{1}$), as shown in Fig. 1 b. This structural change is linked to a semiconductor-semiconductor transition with a small increase of the bandgap from 0.15 eV (ht) to 0.21 eV (lt).
In the same temperature region a change in the magnetic behaviour is observed. Above

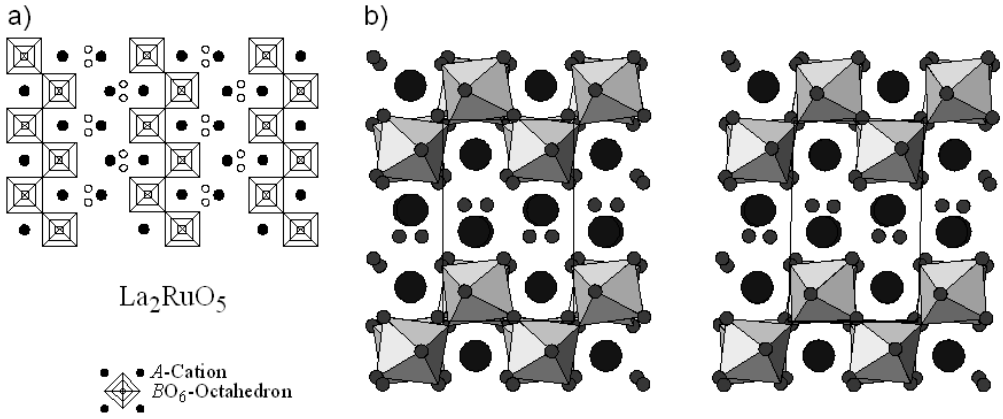

Figure 1: a): Idealized structure of La_2RuO_5, b) Crystal structure of left: ht phase - right: lt phase of La_2RuO_5 derived from neutron diffraction.

160 K the system is paramagnetic with a strong antiferromagnetic coupling, which results in a negative Curie temperature ($\theta_c \approx -177$ K). The measured magnetic moment corresponds to the "spin-only" moment (S = 1) of the Ru^{4+} ion ($\mu = 2.83\,\mu_B$). Below 160 K the magnetic moment nearly disappears, only a weak value below 0.01 emu/mol remains (Fig. 2).
Apossible explanation for the magnetic behaviour was suggested by Khalifah et al. [4]. In their model the spins of the four electrons in the t_{2g} orbitals of the Ru^{4+} ion are coupled with a resulting moment of S = 0. On the other hand LDA and ASW calculations, done by Eyert et al. [5], indicate a completely different scenario: The number of electrons per state, calculated from the density of states, exhibit a spin coupling only in one t_{2g} orbital. The other two spins remain unpaired, giving a S = 1 momentum. To explain the disappearing momentum, the structure transition is taken into account. Here can be seen that the Ru-Ru-bond lengths are not equal like in the ht-phase, but within a RuO_6 zig-zag chain the distances are alternatingly elongated and shortened (Fig. 2), so that two nonequal Ru positions in the structure are present. Additional spin-polarized calculations show a strong antiferromagnetic coupling of these ions resulting in S = 1 dimers. This is comparable to a spin-peierls transition and so called spin ladders are established.
To investigate this theory, substitutions of the cations are currently done. La is substituted by

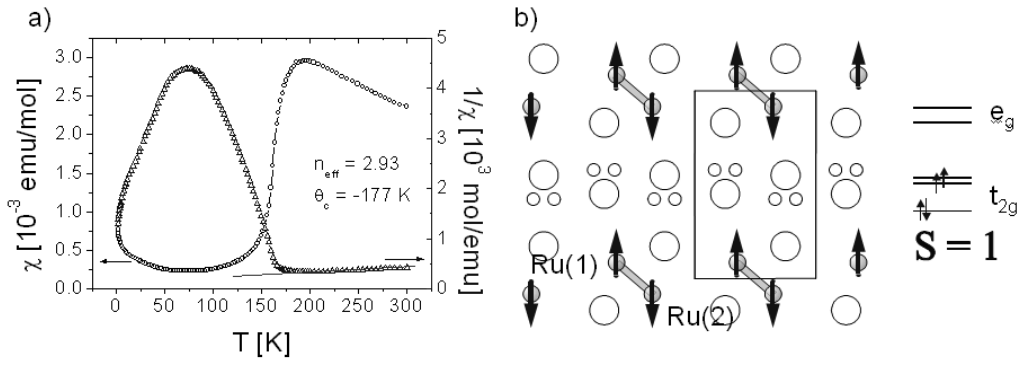

Figure 2: a): Molar magnetic susceptibility of La_2RuO_5, b) Schematc sketch of the Spin-Peierls-like coupling of the local Ru-moments and energy levels of the Ru 4d orbitals.

other Ln elements (Pr, Nd, Sm, Gd, Dy) to determine a possible interaction between the RuO_6 and the LaO_2 layers due to the paramagnetic nature of these ions. So far single phase samples with less than 10 % substitution could be obtained. Another possible approach is to substitute the Ru ions by other 3d and 4d elements. Ti and Zr ions are diamagnetic and Cr, Mn, Fe, Co, Ni ions are paramagnetic and so different influences on the magnetic behaviour in the RuO_6 zig-zag chains are expected. First experiments indicate that no single phase compound could be achieved by classical solid state reactions. Therefore other soft-chemistry methods like e. g. spray pyrolysis are taken into account.
For angular dependend measurements of the magnetic or electrical properties single crystals of La_2RuO_5 are needed. A growth experiment using the floating zone technique with a ten percent excess of Ru (because volatile at very high temperatures) did not yield La_2RuO_5, but led to the discovery of a new material. EDX and thermogravimetry indicate the stochiometry $La_3RuO_{6.95}$. Polycrystalline samples can be synthetisized at temperatures above 1250 °C in air from a molar ratio of 3 : 1 of La : Ru. The structure is not solved yet, but does not match with other La_3RuO_7 structures pulished up to now [6], [7]. For structure solution, diffraction measurements with X-ray, neutrons, synchrotron radiation and electrons were already carried out. First magnetic measurements show an antiferromagnetic coupling with $\theta_c \approx -47$ K and a magnetic moment of 3.50 μ_B, which is slightly lower than the expected spin only value for the Ru^{5+} ion (3.87 μ_B).
In order not to receive only this new material an alternative technique for growing single crystals of La_2RuO_5 has to be applied. This will be a flux method in which $BaCl_2$ is added to the educts to gain small single crystals after heating. These could be used as a seed again for producing a larger crystal in the floating zone experiment.

[1] R. H. Mitchell, Perovskites: Modern and Ancient, Almaz Press, Thunder Bay/Ontario, 2002.

[2] P. Boullay et al., Journal of Solid State Chemistry **170**, 294 - 302, 2003.

[3] S. G. Ebbinghaus, Acta Cryst. C **61**, 96 - 98, 2005.

[4] P. Khalifah et al., Science **297**, 2237 - 2240, 2002.

[5] V. Eyert et al., Phys. Rev. Letters **96**, 256401, 2006.

[6] P. Khalifah et al., Phys. Rev. B **60**, 9573 - 9578, 1999.

[7] P. Khalifah et al., Journal of Solid State Chemistry **165**, 359 - 362, 2002.

16 Stefan Schenk: Density functional theory for lattice models

In solid state physics density functional theory is a standard tool for calculating the electronic structure of real materials. For this task the eigenvalues of the so called Kohn-Sham hamiltonian are commonly interpreted as the electronic bands and for example used to calculate band gaps or Fermi surfaces. However the basic theorems of density functional theory do not guarantee that these calculations give reasonable results. A useful concept for the investigation of these problems has been the consideration of density functional theory on a lattice introduced by Gunnarson and Schönhammer [1, 2].

Groundstate formalism

Density functional theory is derived from the fact that the groundstate minimizes the energie of a quantum mechanical system. This can be used to transform an interacting many-particle Schrödinger equation into a self-consistent one-particle equation which takes much less computational effort to solve. For illustration look at a one-dimensional tight-binding model of spinless fermions. The full Hamiltonian with nearest neighbor interaction reads

$$H = -t \sum_{l=1}^{L} \left(\hat{c}_l^+ \hat{c}_{l+1} + \hat{c}_{l+1}^+ \hat{c}_l \right) + w \sum_{l=1}^{L} \hat{n}_l \hat{n}_{l+1} + \sum_{l=1}^{L} v_l^{\text{ext}} \hat{n}_l. \tag{8}$$

The basic theorem now states that the groundstate energy is a unique functional of the density and that the density is uniquely determined by the potential. The corresponding Kohn-Sham Hamiltonian

$$H_{\text{KS}} = -t \sum_{l=1}^{L} \left(\hat{c}_l^+ \hat{c}_{l+1} + \hat{c}_{l+1}^+ \hat{c}_l \right) + \sum_{l=1}^{L} v_l^{\text{eff}} \hat{n}_l. \tag{9}$$

is then obtained by choosing an effective potential v_l^{eff} such that the groundstate density of the interacting system is correctly reproduced $\langle \hat{n}_l \rangle = \langle \hat{n}_l \rangle_{KS}$. The effective potential v_l^{eff} is the sum of the external potential v_l^{ext}, the Hartree potential $v_l^{\text{Hartree}} = w(\langle \hat{n}_{l-1} \rangle + \langle \hat{n}_{l-1} \rangle)$ and the exchange correlation potential $v_l^{\text{xc}}(\{n_i\})$ which contains the remaining contributions from interaction. The groundstate energy of the interacting system and the corresponding density are then given by

$$E_G = \sum_j \epsilon_j + E_{\text{xc}}(\{n_l\}) - \sum_l n_l (v_l^{\text{xc}} + v_l^{\text{Hartree}}) \qquad n_l = \sum_j |\Phi_j(l)|^2 \tag{10}$$

where the ϵ_j are the eigenvalues of the Kohn-Sham hamiltonian (9) and the Φ_j the corresponding eigenstates. DFT only guarantees that these two quantities yield correct results.
One major problem of DFT is that the exact expression for v_l^{xc} is generally not known so one has to approximate it. One often uses here the local density approximation, where it is assumed that v_l^{xc} only depends on the density of the site l. The potential can then be calculated from exact results of the homogeneous system.
The eigenvalues ϵ_j of the Kohn-Sham hamiltonian are often interpreted as particle-hole excitation energies of the interacting system. That one has to be very careful with such an assumption can be seen easily with a lattice model. There an homogeneous system, where v_l^{eff} is the same on every site, yields the same Kohn-Sham eigenvalues and eigenstates for all interactions w. So the excitation spectrum we get naively from these eigenvalues would be independent of interaction - which is clearly wrong.

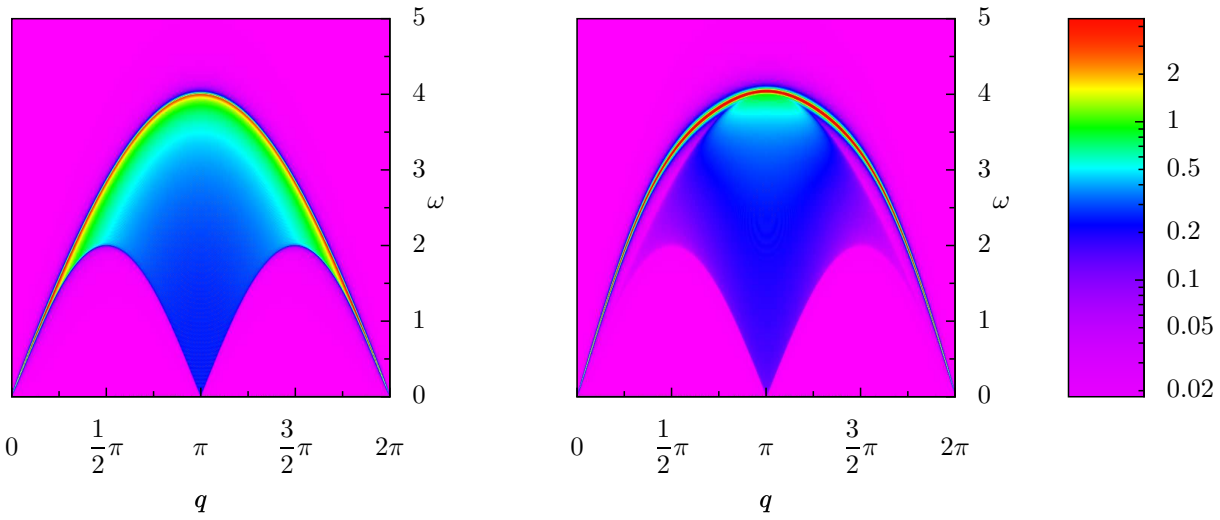

Figure 1: Spectral weight obtained with adiabatic local density approximation for momenta q and excitation energies ω in the noninteracting case (left) and interaction strength $w = 1$. The weight can be read of from the colorscale on the right side

Excitation spectrum

There is an improvement of DFT, called time dependent DFT, which allows to calculate the correct excitation energies [3]. The first step is to calculate the susceptibility from the Kohn-Sham susceptibility. In the homogeneous case this is done for our lattice model by

$$\chi(q,\omega) = \frac{\chi_{\mathrm{KS}}(q,\omega)}{1 + (2w\cos(q) + f_{\mathrm{xc}})\chi_{\mathrm{KS}}}. \tag{11}$$

The excitation energies can then be found as the singularities of the susceptibility. The term $2w\cos(q)$ is the Fourier transform of $\delta v^{\mathrm{Hartree}}/\delta n$. $f_{\mathrm{xc}} = \delta v^{\mathrm{xc}}/\delta n$ stems from the exchange correlation potential. The susceptibility would be exact if one knew the exact expression for f_{xc}. Since we do not have this knowledge we used the the adiabatic local density approximation to calculate χ.
In figure 1 we have plotted $\mathrm{Im}\chi(q,\omega)$ for the noninteracting case on the left and for interaction $w = 1$ on the right. In the left picture one clearly sees the quasiparticle continuum due to electron-hole excitations. In the spectrum on the right hand side one also has this continuum but its spectral weight goes to zero for $q \to 0$. In addition we have a new branch which is dominant for $q \to 0$. This part of the spectrum corresponds to collective excitations. If we compare $\chi(q,\omega)$ with exact results known for our model, we find that the local density approximation exactly reproduces the static susceptibility for $q \to 0$. Another interesting point is that for not too large interactions strengths also the velocity of the collective excitations is in good agreement with exact results.

[1] K. Schönhammer, O. Gunnarson, Phys. Rev. B **37**, 3128 (1987)

[2] K. Schönhammer, O. Gunnarson, R. M. Noack, Phys. Rev. B **52**, 2504 (1995)

[3] M. Petersilka, U. J. Gossmann, E. K. U. Gross, Phys. Rev. Lett. **76**, 1212 (1995)

17 Florian Schrettle: The multiferroic phases of $Eu_{1-x}Y_xMnO_3$

Transition-metal oxides (TMOs) are the subject of intense research-efforts as well in basic and applied solid-state physics for more than 50 years now. The discovery of high-temperature superconductivity about 20 years ago lead to an increased interest in this class of materials. Due to the broad range of physical phenomena appearing in TMOs, e.g. piezoelectricity, ferroelectricity, complex magnetism, colossal magneto-resistance effects, or multiferroic behavior, these compounds have a considerable technological relevance, especially as functional materials in the sector of data storage and processing. With the numerous possibilities to vary the composition and therefore the physical properties of transition-metal oxides, the solid-state physicist finds an enormous field of activity here. The complex physics of transition-metal oxides is a result of the interdependence of the microsscopic degrees of freedom, as e.g. structure, orbitals, spins and charges.

Among the numerous physical phenomena appearing in transition-metal oxides, multiferroic behavior played a very prominent role in recent years. To be called a multiferroic, a compound has to show two or more ferroic properties, like ferromagnetism or ferroelectricity within the same phase. Both order parameters can be strongly coupled. A prominent example for a multiferroic compound is the perovskitic rare-earth manganite $TbMnO_3$ [1].

In these perovskites of the form ABO_3, the structure and therefore the physical properties are strongly influenced by the ratio of the A- and B-site ionic radii. Structural distortions due to mismatch of the ionic radii together with Jahn-Teller type orbital order of the Mn^{3+}-ions on the B-site denote the spin structure of the ground state in these compounds. Along the series of rare-earth manganites from Praseodymium to Holmium, magnetic bond frustration is enhanced and the magnetic structure in the ground state changes from A-type antiferromagnetism in the weakly distorted systems to an incommensurate magnetic phase in the strongly distorted systems (see figure 1) [2].

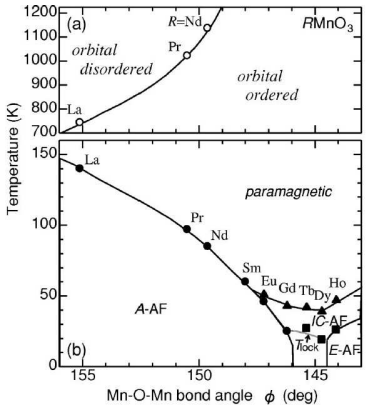

Figure 1: Temperatures of orbital (a) and spin (b) ordering of $RMnO_3$ as function of Mn-O-Mn bonding angle [2].

Within these systems with incommensurate antiferromagnetic structure, compounds with ferroelectric phases are found, e.g. $TbMnO_3$. The origin of ferroelectricity is a spiral modulation

of the spin structure and its interaction with the lattice via the inverse Dzyaloshinskii-Moriya interaction [3, 4].

The doped system $Eu_{1-x}Y_xMnO_3$ represents samples along the series of rare-earth manganites from $EuMnO_3$ over $GdMnO_3$ to $TbMnO_3$. However, in this system, the effects of magnetic rare-earth ions on the multiferroic phases are excluded due to non magnetic A-site ions.
In this talk, experimental results for $Eu_{1-x}Y_xMnO_3$ with Y concentrations $0 \leq x \leq 0.5$ are presented. After discussing the effects of doping on the structure, data for specific heat measurements will be shown. Detailed information on the multiferroic phases of $Eu_{1-x}Y_xMnO_3$ was gained from magnetic susceptibility measurements as well as from measurements of the dielectric constant and the ferroelectric polarisation. Besides the coexistence of ferroelectric polarisation with antiferromagnetic order in a distinguished concentration range, these measurements also reveal the coexistence of a weak ferromagnetic moment and ferroelectric polarisation in $Eu_{0.8}Y_{0.2}MnO_3$. From all these results a detailed (T, x)-phase diagram for $Eu_{1-x}Y_xMnO_3$ was constructed (see figure 2) [5].

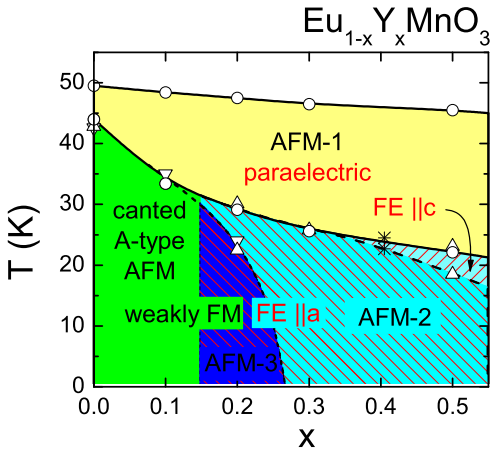

Figure 2: (T, x)-phase diagram of $Eu_{1-x}Y_xMnO_3$ for Y concentrations $0 \leq x \leq 0.5$. AFM-1 denotes the incommensurate antiferromagnetic phase with sinusoidal modulation, while AFM-2 denotes the phase with spiral modulation. AFM-3 finally combines a spiral modulation with a weak ferromagnetic moment [5].

[1] T. Kimura, T. Goto, H. Shintani, K. Ishizaka, T. Arima, and Y. Tokura, Nature(London) **426**, 55 (2003).

[2] T. Kimura, S. Ishihara, H. Shintani, T. Arima, K. T. Takahashi, K. Ishizaka, and Y. Tokura, Phys. Rev. B **68**, 060403 (2003).

[3] M. Kenzelmann, A. B. Harris, S. Jonas, C. Broholm, J. Schefer, S. B. Kim, C. L. Zhang, S.-W. Cheong, O. P. Vajk, and J. W. Lynn, Phys. Rev. Let. **95**, 087206 (2005).

[4] M. Mostovoy, Phys. Rev. Let. **96**, 067601 (2006).

[5] J. Hemberger, F. Schrettle, A. Pimenov, V. Yu. Ivanov, A. A. Mukhin, A. M. Balbashov, and A. Loidl, Phys. Rev. B. **75**, 035118 (2007).

18 Michael Sentef: Magnetization transport in 2D and 3D Heisenberg antiferromagnets

The transport of magnetization through a sample is an issue of high interest and one of the fundamental problems of spintronics research. [1] Typically spintronics devices consist of semiconductors or metals, where one has itinerant charge carriers available. Thus magnetization can be transported via spin-polarized charge currents in these systems.
In insulating magnetic materials, on the other hand, it is also possible to transport magnetization, albeit not via charge currents, but via magnetic excitations like magnons or spinons. The synthesis of quasi-one-dimensional correlated insulators like Sr_2CuO_3 [2] or $CuGeO_3$ has triggered renewed interest in the spin and thermal transport properties of low-dimensional quantum spin systems.
In my talk I present some results of my diploma thesis (2006) which were published in Ref. [3]. The focus is on the transport of magnetization in insulating magnets described by the Heisenberg model, an effective model for localized quantum spins where spin-flip terms allow for dynamic spin excitations like magnons. The central questions of the talk are: (1) How can spin currents be generated? (2) What is the structure of the dynamic spin conductivity?
The natural way to drive a spin current is to apply an inhomogeneous magnetic field, since a magnetic field gradient is the spin transport analogue to a voltage for charge currents. However, there is another possibility to manipulate spin currents if the system exhibits spin-orbit coupling. In this case a time-dependent electric field may also be used to generate a spin current, whose flow direction is perpendicular to the time derivative of the electric field.
In an experiment a magnetization current should be detectable via the electric field which is generated by the moving magnetic dipoles. Possible realizations of such a measurement are proposed in Ref. [4]. The voltage drop for a realistic setup would be of the order of $10^{-13}V$ which indeed appears experimentally feasible.
The transport quantity of interest is the dynamic spin conductivity, which describes how the system reacts to a spin-current driving force. Some results for two- and three-dimensional XXZ Heisenberg antiferromagnets are presented, where "XXZ" means that the coupling of the spins' z components is varied such that one can create and tune an energy gap in the spin excitation spectrum. In the dc limit the spin conductivity of the two-dimensional antiferromagnet shows a nontrivial feature when the energy gap is closed. A central result of this study is shown in Fig. 1. The figure shows the spin conductivity of the 2D antiferromagnet. In contrast to the three-dimensional system, where the spin conductivity vanishes when the gap frequency is approached, the spin conductivity in two dimensions remains finite in the dc limit for the gapless isotropic system.
In the second part of the talk I give a short outlook of what I am planning to do in my PhD thesis "Superconductivity and interface phenomena in correlated electron systems."

[1] The topic of spintronics was recently reviewed by I. Žutić, J. Fabian, and S. Das Sarma, Rev. Mod. Phys. **76**, 323 (2004).

[2] M. Takigawa, N. Motoyama, H. Eisaki, and S. Uchida, Phys. Rev. Lett. **76**, 4612 (1996).

[3] M. Sentef, M. Kollar, and A. P. Kampf, Phys. Rev. B **75**, 214403 (2007).

[4] F. Meier and D. Loss, Phys. Rev. Lett. **90**, 167204 (2003).

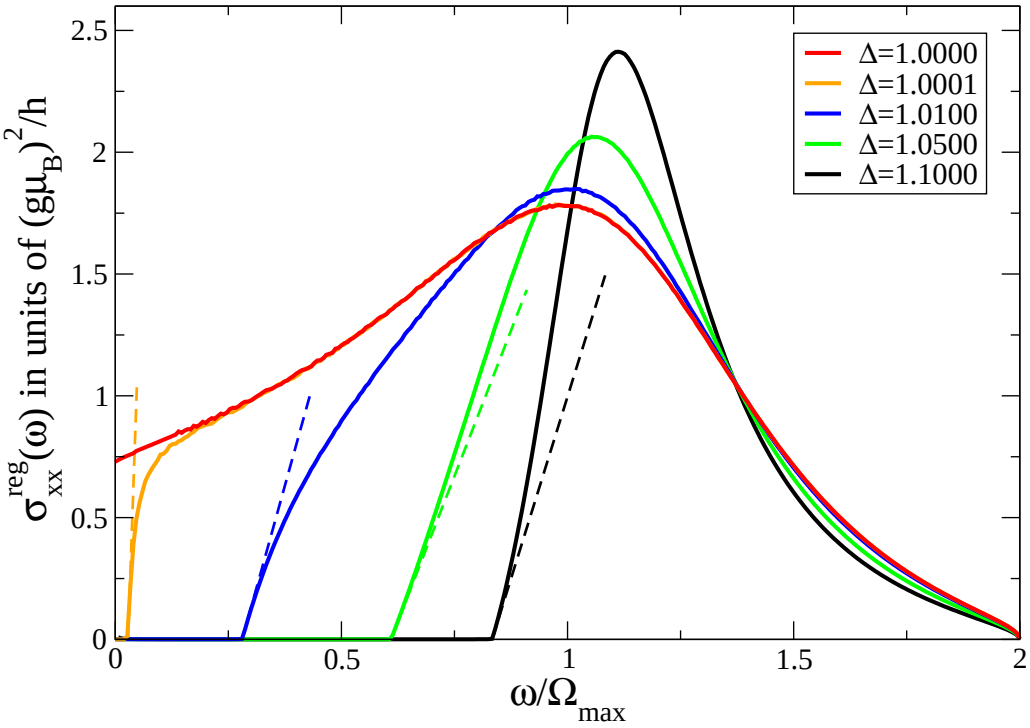

Figure 1: (Color online) Regular part of the longitudinal spin conductivity for interacting magnons (ladder approximation) in two dimensions. Different values of the anisotropy parameter Δ are displayed. The energy gap in $\sigma^{\rm reg}_{xx}(\omega)$ increases with increasing Δ and vanishes for $\Delta = 1$, which corresponds to the isotropic Heisenberg model. The spin conductivity at $\Delta = 1$ remains finite in the dc limit, which is not the case in the three-dimensional system. The dashed lines show analytic expansions around the gap frequencies.

19 Participants

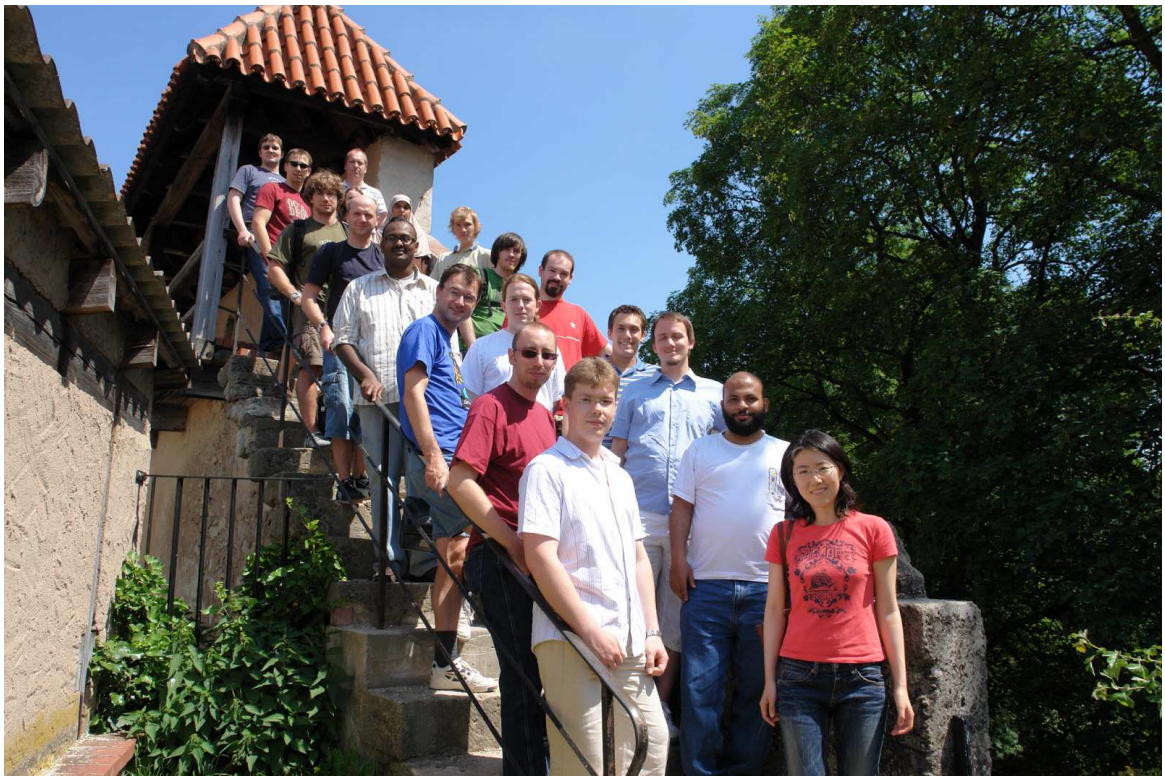

Participant	project
R. Aguiar	D1
M. Eckstein	E6
M. Fadlallah	D2
C. Gorini	D2
R. Hager	E5
F. J. Kaiser	D7
M. Hammida	E1
R. Kaneez	E9
C. Kant	E7
M. Kraus	D5
A. Krimmel	D3
M. Krispin	E2
S. Krohns	E4
H.-J. Lee	E5
G. Obermeier	E2
A. Pashkin	E9
S. Riegg	D1
T. Rudolf	E7
S. Schenk	D2
F. Schrettle	E4
P. Schwab	D2
M. Sentef	E3